



GRADUATE SCHOOL  
EAST TENNESSEE STATE UNIVERSITY

East Tennessee State University  
Digital Commons @ East  
Tennessee State University

---

Electronic Theses and Dissertations

Student Works

---

5-2020

## Ontogenetic and Adult Shape Variation in the Endocast of *Tapirus*: Implications for *T. polkensis* from the Gray Fossil Site

Thomas M. Gaetano  
*East Tennessee State University*

Follow this and additional works at: <https://dc.etsu.edu/etd>

 Part of the [Other Neuroscience and Neurobiology Commons](#), [Paleobiology Commons](#), [Paleontology Commons](#), and the [Zoology Commons](#)

---

### Recommended Citation

Gaetano, Thomas M., "Ontogenetic and Adult Shape Variation in the Endocast of *Tapirus*: Implications for *T. polkensis* from the Gray Fossil Site" (2020). *Electronic Theses and Dissertations*. Paper 3765.  
<https://dc.etsu.edu/etd/3765>

This Thesis - unrestricted is brought to you for free and open access by the Student Works at Digital Commons @ East Tennessee State University. It has been accepted for inclusion in Electronic Theses and Dissertations by an authorized administrator of Digital Commons @ East Tennessee State University. For more information, please contact [digilib@etsu.edu](mailto:digilib@etsu.edu).

Ontogenetic and Adult Shape Variation in the Endocast of *Tapirus*: Implications for  
*T. polkensis* from the Gray Fossil Site

---

A thesis  
presented to  
the faculty of the Department of Geosciences  
East Tennessee State University  
In partial fulfillment  
of the requirements for the degree  
Masters of Science in Geosciences

---

by  
Thomas M. Gaetano  
May 2020

---

Dr. Steven C. Wallace, Chair  
Dr. Christopher C. Widga  
Dr. Richard T. Carter  
Dr. Thomas C. Jones

Keywords: Endocast, Paleoneurology, Tapir, Gray Fossil Site, Telencephalon, Sociality,  
Paleoecology, Sensory Ecology

## ABSTRACT

Ontogenetic and Adult Shape Variation in the Endocast of *Tapirus*: Implications for

*T. polkensis* from the Gray Fossil Site

by

Thomas M. Gaetano

Endocranial morphology provides evidence of sensory ecology and sociality of extinct vertebrates. The Earliest Pliocene Gray Fossil Site (GFS) of NE Tennessee features a conspicuous dominance of skeletal elements belonging to the dwarf tapir, *Tapirus polkensis*. Numerous individuals in one fossil locality often suggests gregarious behavior, but sociality in *T. polkensis* contradicts behavior documented for extant *Tapirus* species. I test *T. polkensis* for variation in sensory and social ecology using computed tomography and 3D digital endocasts from an ontogenetic sequence. I compare the *T. polkensis* endocasts with extant *Tapirus* species using Encephalization Quotients (EQs) and 3D geometric morphometrics. Results show conserved endocast morphology for *Tapirus*, and thus, conserved sensory and social ecology. *Tapirus* behavior is likely consistent for ~5 Ma, and extant *Tapirus* behavior can be inferred for *T. polkensis*. The large number of individuals from the GFS is likely the result of a preservation bias unrelated to gregariousness.

Copyright 2020 by Thomas M. Gaetano

All Rights Reserved

## DEDICATION

This thesis is dedicated to the faculty and staff of the East Tennessee Museum of Natural History for their encouragement and support. This thesis is also dedicated to my family and friends both in and out of the academic community that facilitated a successful academic experience at East Tennessee State University.

## ACKNOWLEDGEMENTS

I acknowledge the Johnson City (TN) Medical Center for conducting the computed tomography scans of the fossil specimens. I also would like to acknowledge my advisor and committee for constructive edits throughout the writing experience. I would like to acknowledge Keila Bredehoft for conducting surface scans of cranial bones that are used in the digital composite skull. I am grateful for the assistance in figure preparation by digital artist and illustrator, Brianna Moore. Dr. Andrew Joyner should be acknowledged for assisting in software installations that facilitated the creation of 3D models and statistical analyses. The entirety of the Department of Geosciences should be acknowledged for the improvements in my critical thinking, technical writing, vertebrate anatomy, and workplace moral. Finally, I acknowledge my classmates and non-student colleagues for support and assistance throughout my graduate school experience.

## TABLE OF CONTENTS

ABSTRACT.....	2
DEDICATION.....	4
LIST OF TABLES.....	7
LIST OF FIGURES.....	8
CHAPTER 1: INTRODUCTION.....	9
CHAPTER 2: METHODS.....	13
Specimens.....	13
Endocasts.....	15
Landmarks.....	17
Statistics.....	18
CHAPTER 3: RESULTS.....	20
Endocast descriptions.....	20
ETMNH 18602 (Figure 5).....	21
ETMNH 12729 (Figure 6).....	25
ETMNH 6821 (Figure 7).....	27
Brain-Body Allometry and EQ.....	29
Principal Components Analysis (PCA).....	32
Discriminant Function Analysis (DFA).....	36
Canonical Variance Analysis (CVA).....	36
CHAPTER 4: DISCUSSION.....	40
CHAPTER 5: CONCLUSIONS.....	51
REFERENCES.....	52
VITA.....	64

## LIST OF TABLES

Table 1. Specimen List .....	13
Table 2. CT Scan Parameters.....	14
Table 3. Landmark Descriptions.....	17
Table 4. <i>Tapirus polkensis</i> Endocast Ratios .....	23
Table 5. Relative Brain Size .....	30
Table 6. Log Transformations and EQ Calculation .....	30
Table 7. EQ Distribution.....	31
Table 8. Principle Component Eigenvalues.....	33
Table 9. Principal Component Coefficients.....	34
Table 10. DFA Result .....	36
Table 11. DFA Classification/Misclassifications .....	36
Table 12. Canonical Variation Among Groups .....	37
Table 13. Mahalanobis Distances .....	37
Table 14. CVA Procrustes Distances.....	37
Table 15. Canonical Coefficients.....	37

## LIST OF FIGURES

Figure 1. Crania and Endocast of ETMNH 12729 .....	16
Figure 2. 3D Endocast of ETMNH 12729.....	16
Figure 3. Landmark Distribution on Example Endocast .....	18
Figure 4. Neural Sensory Information Pathways.....	21
Figure 5. 3D Endocast of ETMNH 18602.....	22
Figure 6. Unified 3D Endocast of ETMNH 12729.....	25
Figure 7. 3D Endocast of ETMNH 6821 .....	28
Figure 8. Brain and Body Mass Regression.....	31
Figure 9. PC2 vs. PC1 Scatterplot .....	32
Figure 10. Principle Component Variance.....	33
Figure 11. PC1 Mean Shape Variation. ....	34
Figure 12. CV1 vs CV2 Scatterplot .....	39

## CHAPTER 1: INTRODUCTION

Functional morphology, as discussed at length by Dunn (2018), is used in paleontology to investigate aspects of behavioral ecology among extinct vertebrates and traditionally is based on analysis of skeletal architecture. However, with increased understanding of the functional properties of the nervous system among extant taxa, it is now possible to apply functional morphology to the nervous system of extinct vertebrates (Torres and Clarke 2018).

Paleoneurology, described as a subdiscipline comprised of paleontology and comparative neurology by Walsh and Knoll (2011), is popular in the age of penetrative 3D scanning. Digital modeling of the endocranial cavity is common practice in paleoneurology and is typically used to study sensory ecology (e.g. Franzosa 2004; Rogers 2005; Sanders and Smith 2005; Rowe et al. 2011; Zelenitsky et al. 2011; Lautenschlager et al. 2012; Boessenecker et al. 2017; Torres and Clarke 2018; Walsh and Knoll 2018; Bertrand et al. 2019), phylogeny and morphology (e.g. Lyras and Van Der Geer 2003; Macrini et al. 2006; Balanoff et al. 2014; Balanoff et al. 2015; Proffitt et al. 2016; Bertrand et al. 2019; Beyrand et al. 2019), and locomotor shifts (Domínguez et al. 2004; Balanoff et al. 2013; Balanoff et al. 2015; Gold and Watanabe 2018; Bertrand et al. 2019). Generally, studies support correlations between behavioral observations of modern vertebrate taxa and the physical nature of the vertebrate brain (Jerison 1985; Rose and Columbo 2005; Shultz and Dunbar 2006; Melhorn et al. 2010; Sakai et al. 2011; Vinuesa et al. 2016; Benson-Amram et al. 2016; Nomura and Izawa 2017 and ref. therein; Ibáñez et al. 2018; Jacobs et al. 2019). Among the morphological and behavioral correlations is the connection between social behavior and the relative volume of the anterior subdivision of the brain (herein referred to as the telencephalon) in vertebrates (Burish et al. 2004; Shultz and Dunbar 2006; Finarelli and Flynn 2009; Sakai et al. 2011; Vinuesa et al. 2016). Research conducted by Shultz and Dunbar

(2006) of ungulate brain size, habitat, and behavioral ecology does include data from two species of tapir, but the sample set is comprised of representatives from all ungulates. Tapirids were minimally represented in the data used by Schultz and Dunbar (2006). Moreover, the endocranial morphology of the extinct *Tapirus polkensis* is an untested aspect of its anatomy, and it can be used to confirm or refute previous notions about the conserved sensory integration and socio-behavioral ecology of the extinct and extant members of the genus.

Evidence of sociality in extinct taxa is usually inferred by the co-occurrence of multiple, articulated skeletons representing a single death event (e.g. Currie 1998; Mihlbachler 2003; Varricchio et al. 2008; Ibiricu et al. 2013; Funston et al. 2016). If the taxon in question exhibits sexual dimorphism, then additional information about the social system is attainable based on the number of males and females (Mead 2000; Mihlbachler 2003). For example, the collection of *Teleoceras major* preserved at Ashfall Fossil Beds from the late Miocene of Nebraska, Antelope County, USA (Tucker et al. 2014) preserves a female-male ratio consistent with herd behavior with a harem-style mating system (Mead 2000). Rarity of such useful fossil megafaunal occurrences calls for additional testing methods of social ecology for extinct taxa like cranial endocast studies. Fortunately, the Gray Fossil Site from the earliest Pliocene of Northeastern Tennessee, Washington County, USA (Schubert and Mead 2011) preserves the largest accumulation of articulated fossil tapir skeletons in the world (Hulbert et al. 2009). Extant members of the genus *Tapirus* are typically considered solitary (Walker 1964; Holden et al. 2003; Schultz and Dunbar 2006; Gilmore 2007; Perez-Barberia et al. 2007; Tobler 2008; Pinho et al. 2014), with the exception of *Tapirus pinchaque* (Downer 1996), so the evidence from Gray suggests a different social ecology because of the unusually high density of articulated individuals. Time-averaging and preservation biases cannot be ruled out as a cause for the large

fossil accumulation, and the dentition of *T. polkensis* lacks prominent sexual dimorphism (Hulbert et al. 2009) which prevents testing for the presence of various forms of gregariousness as in Mead (2000) and Mihlbachler (2003). Therefore, I use an endocranial investigation to test the hypothesis of social ecology variation in *T. polkensis* relative to extant species of *Tapirus*.

Paleocognition, recently defined as the neuro-cognitive processes of fossil species (Uomini and Ruck 2018), is typically applied to ancient humans and the origin human cognition (Logan et al. 2018; e.g. Neubauer et al. 2010; Durrleman et al. 2012; Gunz et al. 2012). Only rarely is cognitive animal research and cranial endocast morphology integrated within vertebrate paleontology, but some examples do exist in avian taxa (e.g. Burish et al. 2004 and Gaetano et al. 2017). There are relationships between variably complex social systems exhibited by ungulates and birds, the cognitive demands of regulating short term relationships in large groups versus long term relationships in a small groups, and gross brain morphology (Shultz and Dunbar 2006). Variation in neuroanatomy results in variation of the cognitive function behind the regulation of observable animal behavior (Butler et al. 2005). It is, therefore, possible to compare brain morphology (derived from the cast of the endocranium) and presume equivalence of neuro-cognitive abilities if there is consistency in their morphology. Burish et al. (2004) for example, investigate fractional volume of the telencephalon in modern Aves and Archaeopteryx, and find similar fractional volumes between the domestic chicken (*Gallus domesticus*) and Archaeopteryx endocast. However, that study only briefly mentions the implications of the similar morphologies as evidence for similar cognitive characteristics and sociality between the two taxa. Gaetano et al. (2017), on the other hand, examine the potential of using extant avians as a modern neuroanatomical analog for inferring mental cognition and behavioral complexity of non-avian maniraptors based on length to width ratios of the telencephalon. In sum, integration of cognitive

animal research into the fossil record is a new field likely because: 1.) it is based on direct observations of behavior (e.g. Hart et al. 2008 and Keeler and Robbins 2011) and 2.) more work is needed to establish neuroanatomical and behavioral correlates on multiple levels of organization from cell structure to gross shape morphology. However, with recent correlates of shape and size of ungulate brains with habitat and social ecology demonstrated by Shultz and Dunbar (2006), comparing endocranial morphology and extrapolating behavioral correlates of *Tapirus* contributes to previous skeletal investigations and is the premise of this study. I use an age sequence to study the relationship between the brain and body size of *T. polkensis*. In addition, I speculate on how interspecific variations may offer a behavioral explanation for the large accumulation of *T. polkensis* at the Gray Fossil Site.

## CHAPTER 2: METHODS

### *Specimens*

Computed tomography (CT) scans from four extant species of *Tapirus* (Table 1) were conducted at University of Texas High-Resolution X-ray CT Facility with a Bio-Imaging Research, Inc industrial grade scanner originally for research by Colbert (1999), with the exception of one previously scanned for Witmer et al. (1999) (Table 1 and 2). Age classifications (Tables 1) were determined using the age categories defined by patterns of tooth eruption developed for (Hulbert et al., 2009); which was also used in a study of tapir skull ontogeny by Moyano and Giannini (2017). Partial to full eruption of the M3 and m3 along with worn DP4 and dp4 to permanently replaced teeth were designated as full adult. Heavy wear in the DP4 and dp4 coupled with complete enclosure of the third molar within the crypt as in MVZ 124091 constituted a sub-adult classification. In addition, three reassembled skulls of *T. polkensis* (Table 1), which are suitable for complete endocasts and represent an ontogenetic sequence, were also CT scanned on helical mode at the Johnson City Medical Center using a GE Healthcare Lightspeed VCT medical CT scanner (Table 2).

**Table 1.** Specimen List

<b>Specimen #</b>	<b>Species</b>	<b>Age Designation</b>	<b>Extinct/ Extant</b>	<b>Wild Caught/Captive Bred + Locality</b>
MVZ 124091	<i>Tapirus pinchaque</i>	Sub-Adult	Extant	Unknown + Colombia
MVZ 124092	<i>Tapirus pinchaque</i>	Infant	Extant	Unknown + Colombia
TMM M-16	<i>Tapirus terrestris</i>	Adult	Extant	Unknown + San Antonio Zoo
FMNH 155691	<i>Tapirus terrestris</i>	Adult	Extant	Unknown
AMNH 80076	<i>Tapirus bairdii</i>	Adult	Extant	Wild Caught + Honduras
AMNH 35661	<i>Tapirus indicus</i>	Adult	Extant	Unknown
ETMNH 18602	<i>Tapirus polkensis</i>	Adult	Extinct	GFS
ETMNH 12729	<i>Tapirus polkensis</i>	Sub-Adult	Extinct	GFS
ETMNH 6821	<i>Tapirus polkensis</i>	Infant	Extinct	GFS

**Table 2.** CT Scan Parameters

<b>Specimen #</b>	<b>Voltage (kV)</b>	<b>Ampere (mA)</b>	<b>Filter</b>	<b>Wedge</b>	<b>% Offset</b>	<b>Integration Time (ms)</b>	<b>Slice Thickness (mm)</b>	<b>Voxel Dimensions (mm)</b>
MVZ 124091	420	4.8	No Filter	Empty Container Wedge	160	32	0.75	0.2197 x 0.2197 x 0.75
MVZ 124092	180	0.133	No Filter	Empty Container Wedge	None	Not Included	2 lines (= 0.208)	0.09473 x 0.09473 x 0.208
TMM M- 16	400	5.19	No Filter	Air Wedge	190	32	1.00	0.5918 x 0.5918 x 1.0
AMNH 80076	410	4.8	No Filter	Air Wedge	190	32	1.00	0.5469 x 0.5469 x 1.0
AMNH 35661	410	4.8	No Filter	Air Wedge	190 (translate offset 3.0)	32	1.00	0.5762 mm x 0.5762 mm x 1.0mm
FMNH 155691	Not Included	Not Included	Not Included	Not Included	-1493	Not Included	1.00	0.7421875 x 0.7421875 x 1.0
ETMNH 18602	120	Not Included	Medium Filter	Not Included	-3024	Not Included	0.65	0.429688 x 0.429688 x 0.65
ETMNH 12729	120	Not Included	Medium Filter	Not Included	-3024	Not Included	0.65	0.429688 x 0.429688 x 0.65
ETMNH 6821	120	Not Included	Medium Filter	Not Included	-3024	Not Included	0.65	0.429688 x 0.429688 x 0.65

### *Endocasts*

Endocasts were created using the CT analysis platform Dragonfly (version 4.1) by Object Research Systems (<https://www.theobjects.com/dragonfly/>) for volume rendering and calculating endocranial volumes using voxel dimensions. The WINDOW LEVELING tool was used on the raw CT scan data to optimize the density contrasts between bone (modern and fossil), matrix, and unoccupied space. Models of the cranial endocast were segmented using the DEFINE REGION and PAINT tools (Figure 1). Incomplete natural endocasts composed of iron concretions partially occupied the endocranial space previously housed by brain tissue and were assigned higher grayscale values because of the greater density compared to empty endocranial space. Iron concretions in the endocranium of the fossil specimens were segmented in yellow for ETMNH 6821 and 12729, and empty endocranial space in blue (Figure 1). The two segments were unified with the UNION tool to create one endocast model (Figure 2). ETMNH 6821 is missing the basioccipital, petrosals, and the exoccipitals, so the skull was digitally composited with 3D models of the missing elements from surface scans of ontogenetically similar specimens. Material selected for the composite included the ETMNH 3699 basioccipital, ETMNH 3697 exoccipitals and ETMNH 20490 petrosals. Surface scan models were created using an Artec Space Spider Structured Light Laser scanner and composited in Microsoft 3D Builder. The digital composite skull of ETMNH 6821 was uploaded into the volume rendering software as a mesh, aligned with the original CT scan, and used to approximate the boundaries of the postero-ventral endocast. Contour meshes were generated from the endocast models, a smoothing algorithm with one iteration was applied, and the meshes were uploaded as ply files into Landmark Editor 3.6 for 3D landmark placement (developed by the Institute for Data

Analysis and Visualization and the University of California, Davis). This software is no longer supported by the original developers.

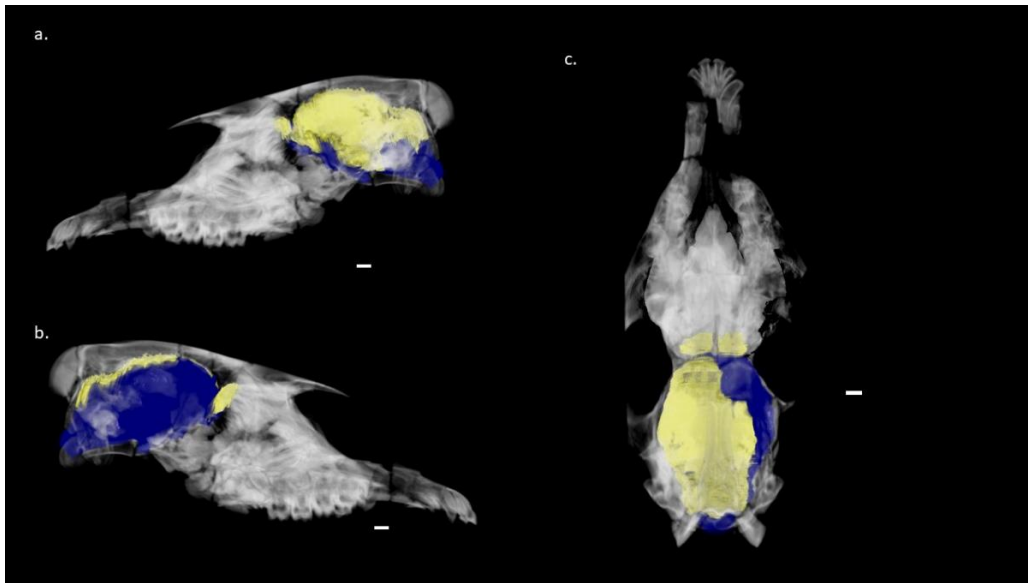


**Figure 1.** Crania and endocast of ETMNH 12729 in a.) left lateral, b.) right lateral, and c.) dorsal view. Crania is rendered transparent, iron-rich concretion is rendered yellow, and digital endocast is rendered in blue. Scale bars = 1 cm.

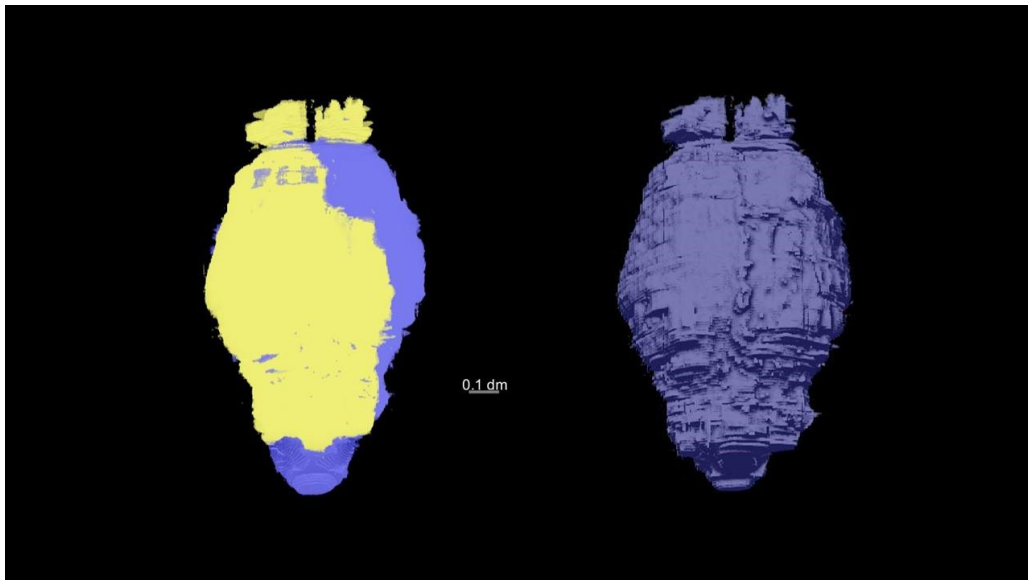


**Figure 2.** 3D endocast of ETMNH 12729 in dorsal views. The left model represents the two components of the endocranial volume with the iron-rich concretion rendered yellow and the digital endocast rendered blue. The right model represents the endocranial model after unifying the two components. Scale bar = 0.1 dm.

## Landmarks

13 homologous landmarks (Table 3) were placed on the cranial endocasts for a 3D geometric morphometric approach to capture shape variation across species of comparable developmental stages. Landmark types follow Bookstein (1991). Landmarks 1 and 2, 4-11, and 13 were taken from a comparative study of procyonid endocasts by Ahrens (2014). However, the olfactory bulbs are separated in the *Tapirus* endocasts (Figure 3) unlike the joined left and right olfactory bulbs of the procyonid endocasts from Ahrens (2014). Therefore, landmark 3 was placed on the *Tapirus* endocast to capture the width of the olfactory bulb. Landmark 12 was added to capture the intersection of the frontal, temporal, and piriform lobes and is thus considered a type I landmark. Landmark Editor 3.6 was used to place the landmarks onto the endocast surface (Figure 3), and the exported coordinate data was imported into MorphoJ version 1.07a software for statistical analysis (Klingenberg 2011).

**Table 3.** Landmark Descriptions

<b>Landmark</b>	<b>Description</b>	<b>Type</b>
1	Rostral Terminus of Right Olfactory Bulb	3
2	Right Lateral Terminus of Right Olfactory Bulb	3
3	Left Lateral Terminus of Right Olfactory Bulb	3
4	Dorsal Terminus of Right Olfactory Bulb	3
5	Caudal Constriction at Dorsoventral Midpoint of Right Olfactory Bulb	2
6	Terminus Right Piriform Lobe Ventral Protuberance	2
7	Hemispherical intersection with Cruciate Sulcus	1
8	Caudal Dorsal Maxima of Vermis Curve	2
9	Caudal Ventral Terminus of Vermis	3
10	Caudal Midline Terminus Between Left and Right Occipital Lobes	3
11	Right posterolateral terminus of Internal Acoustic Meatus	3
12	Intersection of Left Frontal, piriform, and temporal Lobes	1
13	Tip of Pituitary Gland Protuberance	2

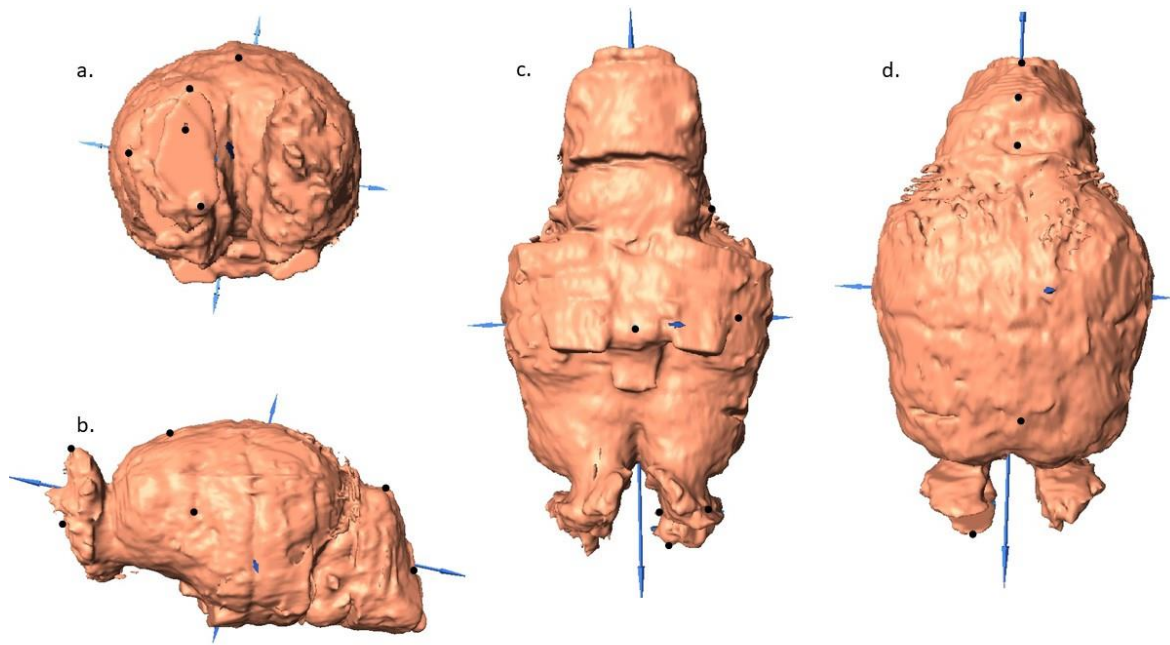


**Figure 3.** Landmark distribution across the FMNH 155691 (*Tapirus terrestris*) endocast in a.) anterior, b.) left lateral, c.) ventral, and d.) dorsal views. 13 landmarks used in total (black points).

### *Statistics*

Landmarks were transformed with a Procrustes Fit in MorphoJ. Generated shape coordinates were then analyzed with Principle Components Analysis (PCA), Discriminant Function Analysis (DFA), and a Canonical Variance Analysis (CVA) in MorphoJ. Endocasts were classified Extant or Extinct for the DFA and Infant, Sub-Adult, or Adult for the CVA.

An adult brain-body size allometric equation was calculated for extant species of *Tapirus* using the body mass calculations from Hulbert et al. (2009) and measured brain volumes from the endocranial models created for this study. Following Iwaniuk and Nelson (2002) and Burger (2018, personal communication), endocranial volume was converted to grams using a brain tissue density (1.036 g/mL). Additionally, published brain and body mass data were included from a larger study by Burger et al. (2019) were included to create a brain-body size allometry

that was unique to the genus *Tapirus*. Extant adult brain and body mass data were plotted and regressed using a power trendline to produce an allometric equation that matched the format in Burger et al. (2019). Expected brain mass was calculated using the brain-body mass allometric relationship derived in this study. Finally, the expected brain mass for *T. polkensis* was calculated by inserting its body mass estimate from Hulbert et al. (2009) into the brain-body mass regression. Observed and expected brain mass was log transformed, and encephalization quotients (EQs) were calculated as the ratio of observed to expected brain mass.

## CHAPTER 3: RESULTS

### *Endocast descriptions*

Unless stated otherwise, all descriptions below use neurologic terminology, but refer to the cranial endocast structures following the methods of Sampson and Witmer (2007). Endocasts are accepted as a proxy for mammalian brains because there is a reduction of non-neural soft tissues occupying the braincase and is supported by impressions of vasculature, cerebral-cortical folding, or both on mammalian endocasts (Walsh and Knoll, 2011 and sources within). The endocast is digitally produced from an adult specimen of *Tapirus polkensis* (ETMNH 18602) and described following the methods of Macrini et al. (2007a) who first presented basic metrics followed by the details of the three regions of the brain (forebrain, midbrain, hindbrain). Descriptions flow from the anterior regions to the posterior and are divided into four sections: overall, forebrain, mid-brain, and hindbrain. An example of boundaries between these regions are illustrated for a basal mammal in Macrini et al (2007a) and sensory input and output pathways can be found in a basal and derived mammalian form in Rowe et al. (2011) and Iyengar et al. (2017) (Figure 4). The conserved sensory integration pathways across basal and derived mammals (Figure 4) provided the basis to interpret the qualitative descriptions in terms of sensory ecology.

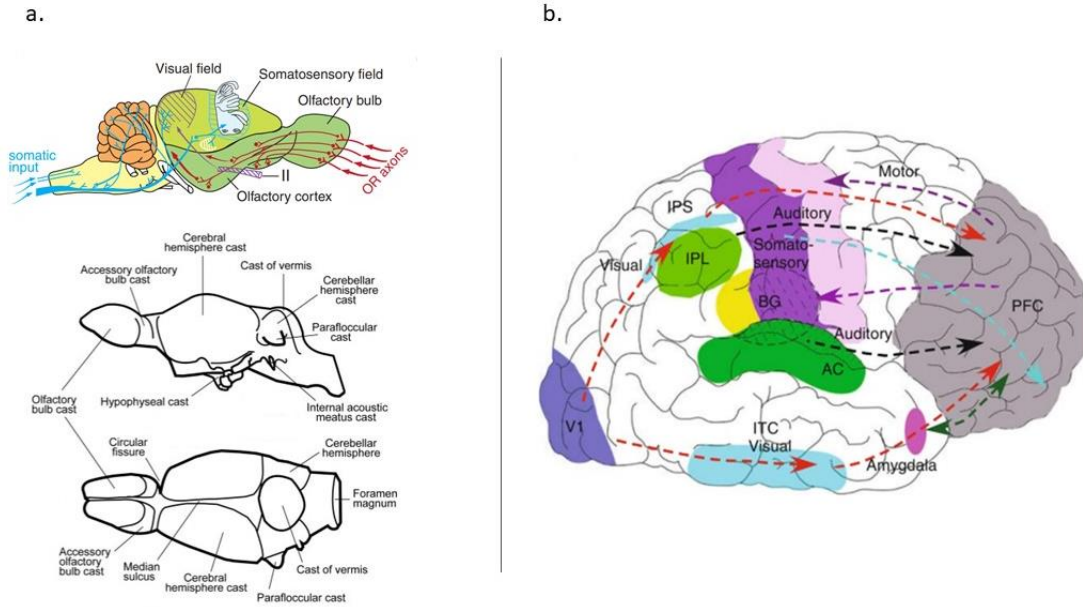


**Figure 4.** Schematic drawings of sensory information pathways through the brain of a basal mammal (a) and a derived mammal (b). Abbreviations: AC, auditory cortex; BG, basal ganglia; IPL, inferior parietal lobule; IPS, intraparietal sulcus; ITC, inferotemporal cortex; PFC, prefrontal cortex; V1, primary visual cortex. Arrows indicate interregional connections between areas colored in green, blue, purple, light purple, yellow, grey, and pink. Modified from Rowe et al. (2011), Macrini et al. (2007a), and Iyengar et al. (2017).

*ETMNH 18602* (Figure 5)

*ETMNH 18602* is the focus of description given its excellent preservation and minimal braincase concretions. However, brief descriptions of the endocast from *ETMNH 12729* and *ETMNH 6802* are also included to provide a qualitative basis for shape change through ontogeny in the discussion.

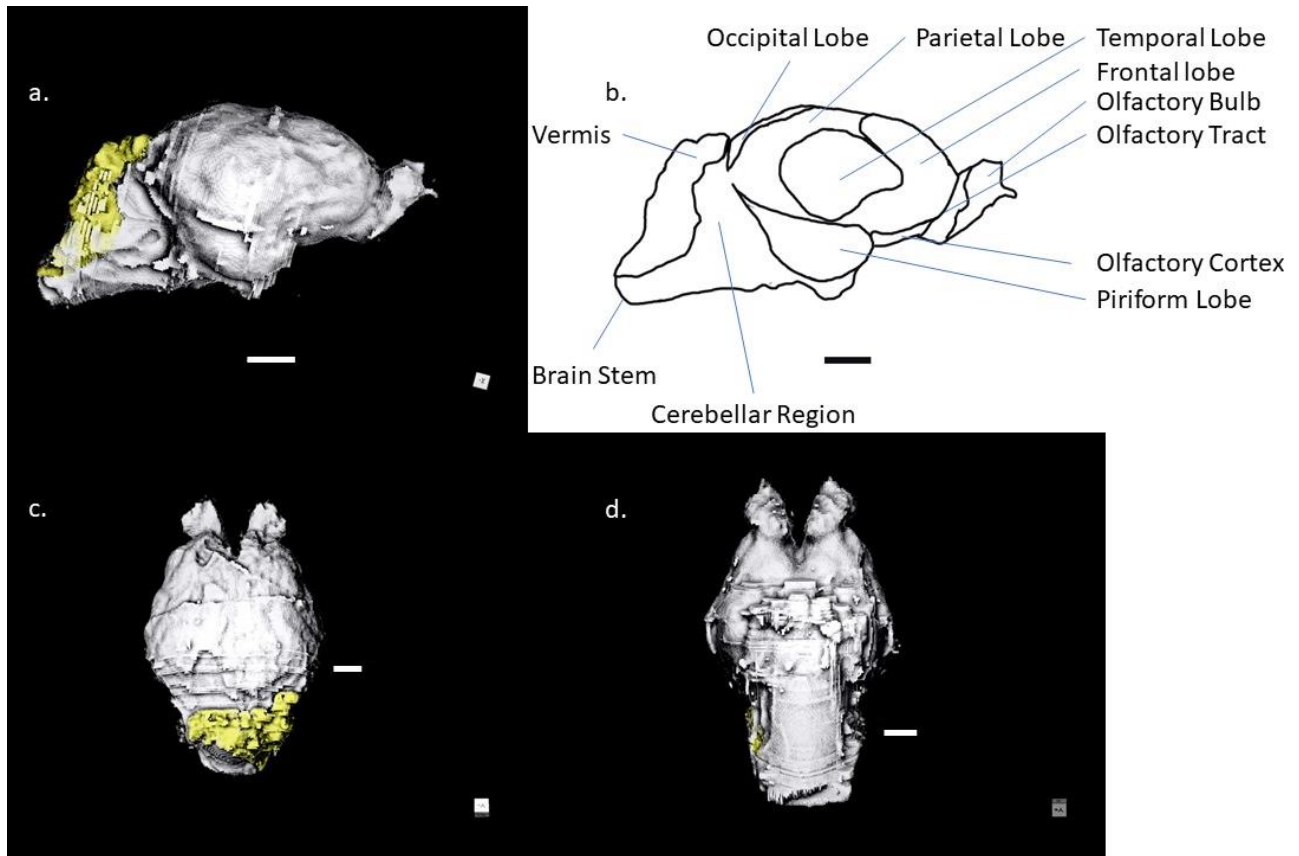


**Figure 5.** Digital endocast of ETMNH 18602 in a.) right lateral, c.) dorsal, and d.) ventral views. 5b.) represents visible regions of the brain in right lateral view. Yellow segmented regions indicate iron concretion that denotes the natural portion of the endocast and the vermis structure. Grey regions indicate hollow space in the endocranium. Scale bars = 1 cm.

*Overall Description.* Width to length ratio in dorsal view is 0.81 (Table 4). Height to length ratio in lateral view is 0.67. In dorsal view the endocast is pear-shaped and is widest at the parietal/temporal region. The olfactory region is separated into two distinct lobes that do not connect until the mid-cerebral region. In lateral view, the dorsal surface of the telencephalon is flat and slopes downward posteriorly and anteriorly. Posteriorly, the dorsal surface flattens until the posterior extent of the telencephalic region. The dorsal surface of the vermis flattens slightly and a posterior angle of approximately  $120^\circ$  leads to the foramen magnum. Dorsal and posterior regions are defined by iron concretions.

**Table 4.** *Tapirus polkensis* Endocast Ratios

	<b>Width/length</b>	<b>Height/length</b>
Infant	0.84	0.57
Sub-adult	0.75	0.75
Adult	0.81	0.67

*Forebrain.* Olfaction is divided into two distinct bulbs. Cribiform plates are deflected laterally from the mid-line (Figure 5c). Olfactory bulbs are short, wide, and flat, whereas the accessory bulb is indiscernible beneath the main olfactory bulbs. Posterior to each bulb there is a rapid constriction that is referred to as the circular fissure in Macrini et al. (2007a). Olfactory tracts posterior to the circular fissure are short with a slight angle towards the medial endocast. Division of the olfaction persists through the frontal lobe. Boundaries of the frontal lobes are discernible and indicate a dorsal ventral position of the anterior endocast immediately posterior to the olfactory tracts (Figure 5a,b). The region is small, ovular, and situated rostrally to the olfactory tracts and dorsally to the olfactory cortex. Olfactory cortex is medio-ventral to the frontal lobe and posterior to the olfactory tracts in ventral view (Figure 5d). Cerebral hemispheres appear mostly lissencephalic, or without gyri and sulci. However, the surface is not smooth, and there are five identifiable major lobes in lateral view (Figure 5b). Domestic equids, another clade within Perissodactyla, have cerebral-cortical folding whereas basal mammals do not (Macrini et al. 2007b; König et al. 2009). Therefore, given the closer phylogenetic relationship of *Tapirus* to Equidae, it is likely that there is some degree of cerebro-cortical folding in the brain of *T. polkensis* that does not leave impressions on the inner surface of the endocranium in the adult stage.

There is a median sulcus that divides the cerebral hemispheres in dorsal view (Figure 5c). Also, the hemispheres truncate perpendicularly to the median sulcus at the posterior forebrain. Other visible lobes in lateral view of the endocast, in addition to the frontal lobe, includes the

temporal, parietal, pyriform, and occipital lobes and the olfactory cortex (Figure 5a,b). Dorsal boundary of the frontal lobe in right-lateral view forms a J-shape (Figure 5b). Progressing postero-laterally, the temporal lobe is most defined in right-lateral view and forms the widest portion of the endocast in dorsal view (Figure 5b,c); it is dorsally broad in right-lateral view and narrows ventrally forming a rounded triangular shape (Figure 5a,b). The parietal lobe is defined well enough for an identification on the dorso-posterior roof of the endocast (Figure 5b,c); in dorsal view it has a large surface area. The boundary of the parietal lobe is high and aligned with the dorsal extent of the temporal lobe..

*Midbrain.* The hypophyseal cast, which corresponds to the pituitary gland (Hönig et al., 2009), is well-defined on the ventral surface of the endocast and is posterior to the optic chiasm (Figure 5d). Points at which the oculomotor nerve and the maxillary nerve are joined with the endocast, prior to being encased in ossified foramen, are visible in the mid brain region. Much of the mid-brain components are internal and include elements like the thalamus so the description of these brain regions is limited.

*Hindbrain.* Hindbrain is rounded at the osseous tentorium, and the cerebellar hemispheres appear distinguishable in dorsal view as two parallel ridges lateral from the vermis cast (Figure 5c). Dorsal and right-lateral portions of the vermis are defined by a naturally formed endocast composed of iron-rich concretion. The left lateral side of the hindbrain features a cast of the internal acoustic meatus (Figure 4), but no apparent cast of the paraflocculus (Figure 5a). A cast of the ventral part of the pons is defined on the ventral hindbrain by a small, rounded bulge that is anterior to the brain stem cast and foramen magnum (Figure 5d). The right abducent nerve, which travels around the right lateral side of the pons, left an impression of the ventral hindbrain

(Figure 5d). No other nerve foramina casts can be confidently identified by the author on these endocasts. Shape of the foramen magnum is oval with the long axis on the transverse plane.

*ETMNH 12729* (Figure 6)

*Overall Description.* Endocast width to length ratio in dorsal view is 0.75 and the height to length ratio in lateral view is also 0.75 (Table 4). Anterior regions of the endocast are more rounded and bulbous in left-lateral view than that of ETMNH 18602 and a large concretion comprising a greater portion of the endocast model than the ETMNH 18602 endocast situated on the left lateral side (Figure 6). Posteriorly, the concretion projects towards the right of the midline and defines the dorsal half of the hind brain region. Internally, the boundary between the naturally formed partial endocast and the empty endocranial space begins dorsally from right lateral side and ends ventrally on the left lateral side.

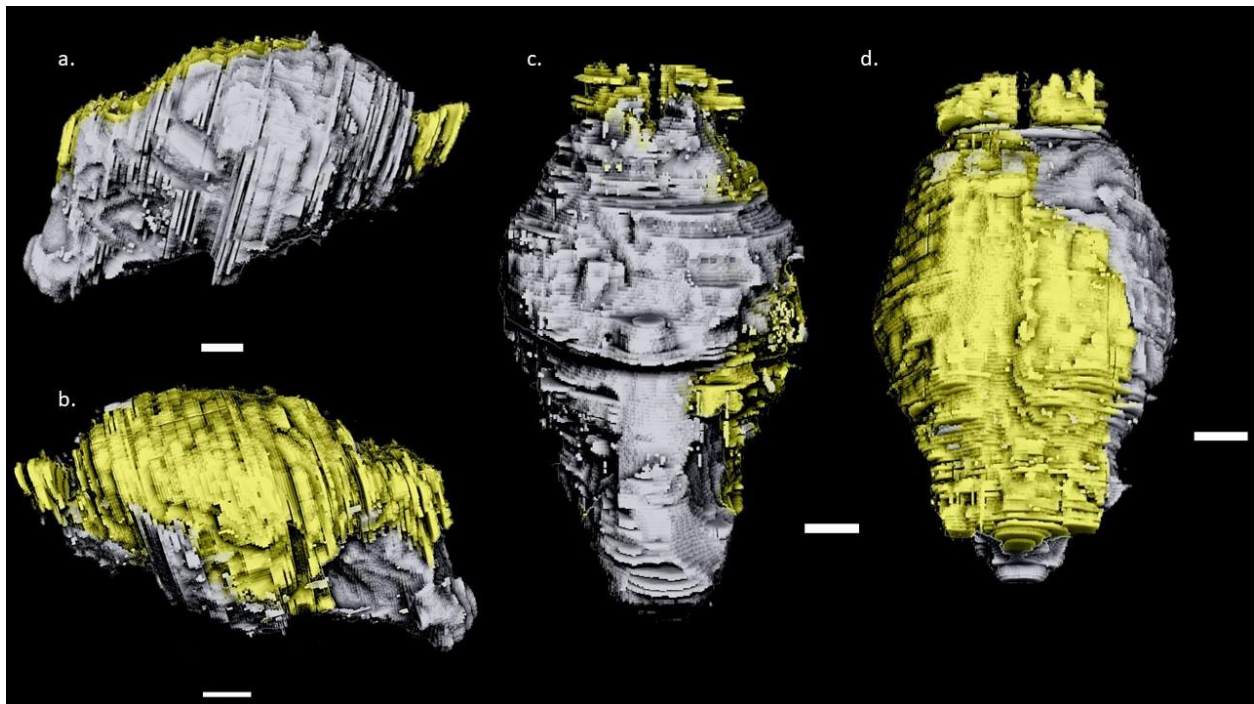


**Figure 6.** Digital endocast of ETMNH 12729 in a. right lateral, b. left lateral, c. ventral, and d. dorsal views. Yellow segmented regions indicate iron concretion that denotes the natural portion of the endocast. Scale bars = 1 cm.

*Forebrain.* Olfactory bulbs are separated and shifted medially relative to the ETMNH 18602 endocast (Figure 6c,d). Both left and right bulbs are naturally formed casts of the same iron concretion mentioned previously. Endocast surface is without gyri and sulci as in ETMNH 18602. Olfactory tracts are short, and the left and right prefrontal and olfactory cortices are not separated in contrast with ETMNH 18602 and other endocasts in this study (Figure 6c). Posterior to the olfactory bulb, the frontal lobe is more anteriorly truncated and rounded than ETMNH 18602. Dorsal roof of the endocast is flat as in ETMNH 18602 (Figure 6 a,b). In dorsal view, this flattening in lateral view is the result of two symmetrical projections on both sides of the hemispherical midline near the occipital lobe area of the posterior telencephalon (Figure 6d). Following the midline of the cerebral hemispheres shows curvature in the dorsal surface of the forebrain.

The boundary between the temporal lobe and the frontal lobe forms a J-shape as in the ETMNH 18602 endocast in lateral view (Figure a,b), and the olfactory cortex is not discernable in ventral view (Figure 6c). In dorsal view, the cruciate sulcus is divided into two halves at the midline with the naturally formed endocast forming the left side and digitally modeled endocast forming the right side (Figure 6d). The temporal lobe boundary on the left lateral side (defined by naturally formed casts in Figure 6b) is pear shaped and the left pyriform lobe is ventral to the temporal lobe. Parietal lobe regions are defined by the concretions on the left and right hemispheres, and the occipital lobe regions are posterior to the temporal lobes (Figure 6b). Surfaces are not smooth as in ETMNH 18602, so the shapes cannot be described in the same detail and the boundaries between the regions are not as clearly defined.

*Midbrain and Hindbrain.* Within the midbrain, hypophyseal cast is well defined, but truncates suddenly in the anterior direction (Figure 6c). The optic chiasm shifts in a right lateral

direction in ventral view, and no other major features of the midbrain are discernable in the endocast model (Figure 6c). Features of the hindbrain include iron concretion along the dorsal and left dorsal section of the vermis (Figure 6a,b,d). There is no discernible cast of the paraflocculus present on the lateral hind brain (Figure 6a,b). The right lateral section of the vermis is digitally modeled and shows a two-pronged internal acoustic meatus at the dorso-ventral midpoint (Figure 6a). The angle of the posterior vermis and the brain stem through the foramen magnum is steep. Brain stem is rounded in contrast to the oval-shape in ETMNH 18602 (Figure 6c).

#### *ETMNH 6821* (Figure 7)

*Overall Description.* Endocast width to length ratio in dorsal view is 0.84 and the height to length ratio in lateral view is 0.57 (Table 4). In dorsal view it appears more rounded than that of the ETMNH 18602 and 12729 endocasts (Figure 7c). Moreover, it is more constricted in the anterior-posterior aspect than either of the previous endocasts (Figure 7). Iron concretion forms a natural cranial endocast in the antero-ventral region and includes the olfactory bulbs (Figure 7a,d). Features defined by the naturally formed endocast include the optic chiasm, oculomotor and maxillary nerve junctions, olfactory cortices, pyriform lobes, and the ventral extent of the temporal and frontal lobes (Figure 7d). Internally, the natural portion of the endocast forms a bowl shape that is settled in the ventral endocranium. In contrast, the natural portion of the ETMNH 12729 endocast is positioned on the left lateral side of the endocranium extending from the dorsal surface to the ventral aspect of the left lateral side (Figure 6). Dorsal roof of the endocast is more curved, but three distinct angles that flatten between the anterior and posterior telencephalon make it consistent with the previous endocasts (Figure 7a). The endocast shows some gyri and sulci that appear on the dorsal surface of the telencephalic region (Figure 7c).

Anterior forebrain of ETMNH 6821 is not separated as in ETMNH 18602 and the extant endocasts, although in ventral view the olfactory cortex does form two distinct features that correspond with the left and right hemispheres (Figure 7c,d).

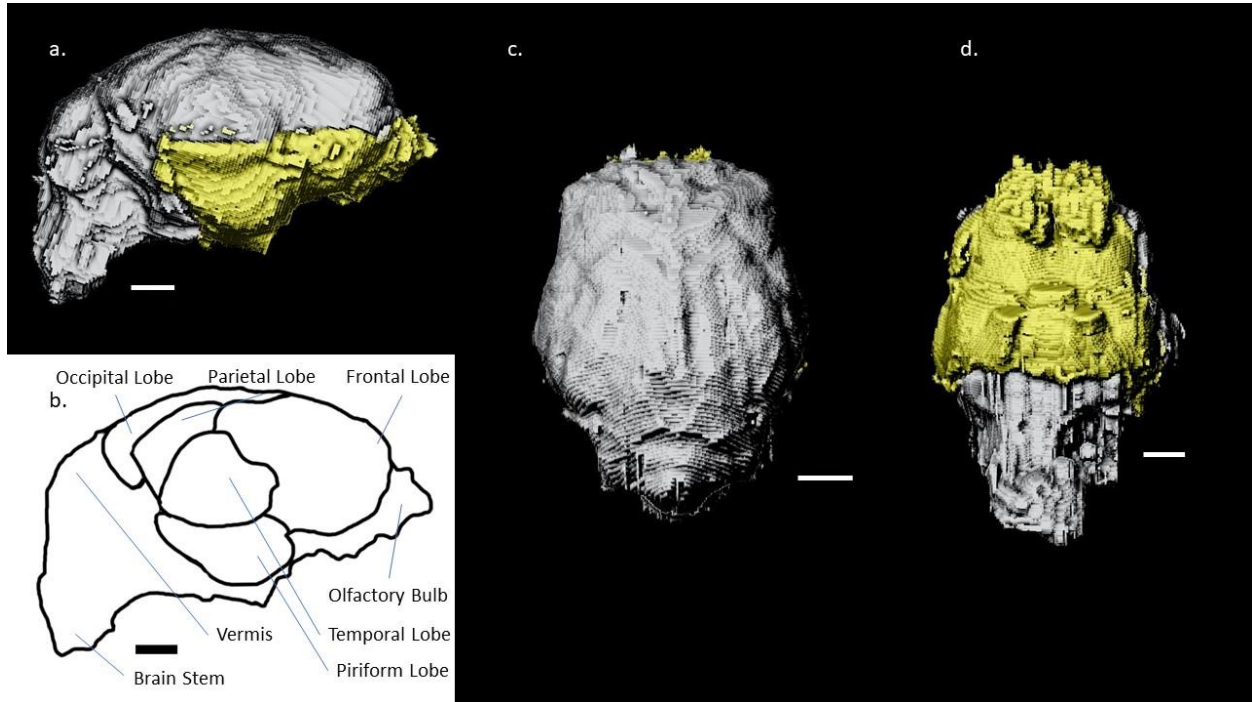


**Figure 7.** Digital endocast of ETMNH 6821 in a. right lateral, c. dorsal, and d. ventral views. 7b represents visible regions of the brain in right lateral view. Yellow segmented regions indicate iron concretions that denote the natural portion of the endocast. Scale bars = 1 cm.

*Forebrain.* The anterior olfactory bulb surfaces project downward, and the bulbs are positioned more ventrally compared to their position on ETMNH 18602 (Figure 7a,b). Olfactory bulbs are medially constricted, as is the condition of the olfactory bulbs in the ETMNH 12729 endocast, and olfactory tracts are reduced such that the bulbs appear in direct contact with the frontal lobe (Figure 7a,d). Frontal lobes are larger relative to the whole telencephalon and in right lateral view forms a subtriangular shape (Figure 7b). Additionally, the telencephalic region appears to comprise a greater portion of the entire endocranial volume (Figure 7). Cruciate sulcus is posteriorly shifted compared to ETMNH 18602 (Figure 7c). The temporal lobes are

large and round and the boundaries to the frontal, pyriform, parietal, and occipital lobes are well defined (Figure 7b). Pyriform lobes are ventral to the temporal lobe in right lateral view and the parietal lobe is large, flat, and dorsally situated posterior to the frontal lobe (Figure 7b,c). Finally, the occipital lobes are small and posterior to the temporal lobes along the dorso-ventral midpoint (Figure 7b).

*Midbrain and Hindbrain.* Within the midbrain, the hypophyseal cast is reduced in comparison to the ETMNH 18602 and 12729 endocasts (Figure 7d). Optic chiasm is situated posteriorly to the olfactory cortex and maxillary and oculomotor nerves are well defined and medial to the pyriform lobes (Figure 7d). The hindbrain region features a ridge that is present at the junction of the natural and digital endocast in ventral view (Figure 7d). The vermis occupies a smaller portion of the total endocast size and is aligned with the dorsal surface of the forebrain region (Figure 7a). Vermis drops steeply into the brain stem, which is oval shaped at the as in the ETMNH 18602 endocast (Figure 7a,d), and the left lateral side of the hind brain is flattened compared to the right lateral side (Figure 7d).

#### *Brain-Body Allometry and EQ*

The power regression of the brain-body mass data is  $y = 0.0005x^{1.0781}$  with an  $R^2$  value of 0.4537 (Figure 8). Expected brain mass for the extant and extinct species is calculated by inserting the body mass data into the power regression of the data from extant species (Tables 5 and 6). EQ is calculated as a ratio between the log-transformed expected and observed brain mass for all specimens in this study. Based on the data from the extant species, *T. polkensis* EQ is ~1.06 and cannot be considered a statistical outlier with a Z score of ~0.98 (Table 7). The mean and median EQ value is ~1.00 and the coefficient of variation is ~6.36 (Table 7). *Tapirus bairdii* relative brain size deviates the most from the EQ distribution with a brain mass value of

0.85 g and an EQ of 0.86 (Table 5 and 6). However, it cannot be excluded as an extreme statistical outlier with a Z score of  $\sim -2.22$  (Table 7).

**Table 5.** Relative Brain Size

<b>Species + Data Source</b>	<b>Body Mass (g)</b>	<b>Brain Volume (cm<sup>3</sup>)</b>	<b>Brain Mass (g)</b>
<i>Tapirus indicus</i> AMNH 35661	352336	344.07	356.45
<i>Tapirus indicus</i> Boddy et al., 2012	201000	255.79	265
<i>Tapirus bairdii</i> AMNH 80076	223000	272.23	282.03
<i>Tapirus bairdii</i> Boddy et al., 2012	142600	82.05	85
<i>Tapirus terrestris</i> TMM M-16	184000	294.38	304.97
<i>Tapirus terrestris</i> Boddy et al., 2012	160000	174.23	180.5
<i>Tapirus terrestris</i> FMNH 155691	184000	272.59	282.40
<i>Tapirus pinchaque</i> MVZ 124091	156923	244.33	253.13
<i>Tapirus polkensis</i> ETMNH 18602	125000	272.59	209.74

**Table 6.** Log Transformations and EQ Calculation

<b>Specimen</b>	<b>Log Body Mass</b>	<b>Log Brain Mass</b>	<b>Expected Brain Mass (g)</b>	<b>Log Expected Brain Mass</b>	<b>EQ</b>
<i>Tapirus indicus</i> AMNH 35661	5.55	2.55	477.69	2.61	0.95
<i>Tapirus indicus</i> Boddy et al. (2012)	5.30	2.42	260.82	2.40	1.00
<i>Tapirus bairdii</i> AMNH 80076	5.35	2.45	291.73	2.44	0.99
<i>Tapirus bairdii</i> Boddy et al. (2012)	5.15	1.93	180.15	2.26	0.86
<i>Tapirus terrestris</i> TMM M-16	5.26	2.48	237.12	2.36	1.05
<i>Tapirus terrestris</i> Boddy et al. (2012)	5.20	2.26	203.95	2.31	0.98
<i>Tapirus terrestris</i> FMNH 155691	5.26	2.45	237.12	2.30	1.03

**Table 6.** Log Transformations and EQ Calculation

Specimen	Log Body Mass	Log Brain Mass	Expected Brain Mass (g)	Log Expected Brain Mass	EQ
<i>Tapirus pinchaque</i> MVZ 124091	5.20	2.40	199.73	2.21	1.04
<i>Tapirus polkensis</i> ETMNH 18602	5.26	2.45	156.30	2.36	1.06

**Table 7.** EQ Distribution

Mean=	1.00
Median=	1.00
Variance=	0.004
Stand Dev=	0.06
Range=	0.20
Q1=	0.96
Q3=	1.05
IQR=	0.08
Coefficient of Variation	6.36%
Z score <i>T. polkensis</i> =	0.98
Z score <i>T. bairdii</i> =	-2.22

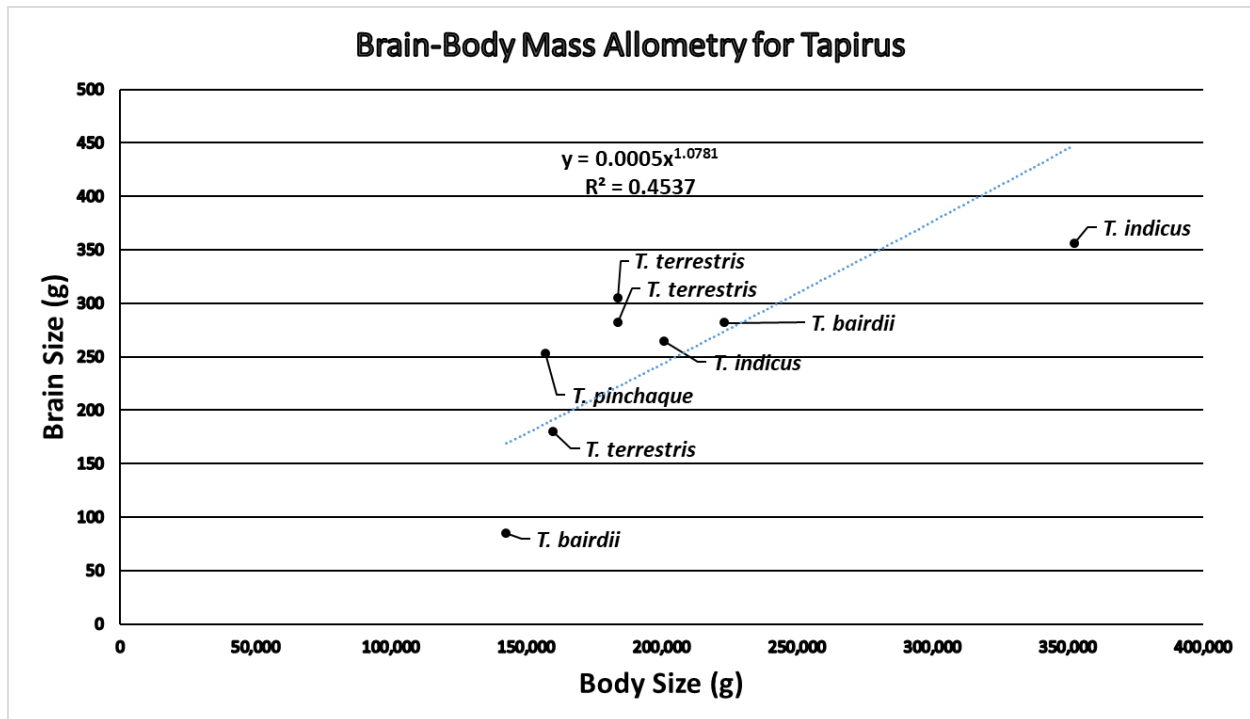


**Figure 8:** Power regression of Brain and Body Mass data for the extant genus members. Power regression documents the brain-body size allometric relationship for the genus *Tapirus* based on data from extant species.

### Principal Components Analysis (PCA)

MVZ 124092 did not preserve the cribiform plate or the endoturbinates, so Landmarks 1-5 are not included in the analysis. The scatterplot graph for PC1 and PC2 shows the infant MVZ 124092 separating from the group (Figure 9). Eigenvalues and the percent variance attributable to each is summarized in Table 8. Variance for the first three principal components are 70.952%, 11.434%, and 5.771%, respectively (Figure 10). Shape changes of PC1 result in landmark shift vectors in a lollipop diagram in which the average landmark position is shown by the filled in circles and the direction of average variation is shown by the vectors (Figure 11). Total variance is ~0.048, and the variance of the eigenvalues is ~0.00004. Eigenvalue variance scaled by total variance is ~0.015 and is 0.51 when scaled by the total variance and number of variables. Throughout all calculations of eigenvalue variances, the dimensionality used is 32, and there are fewer PCs than dimensions in shape space (Table 8). The potential reasons are as follows: 1.) the degrees of freedom are less than the shape dimensionality (sample size, etc.), and 2.) there is complete integration in the data. Therefore, these results require cautious interpretation. The principle component coefficients are reported in Table 9.

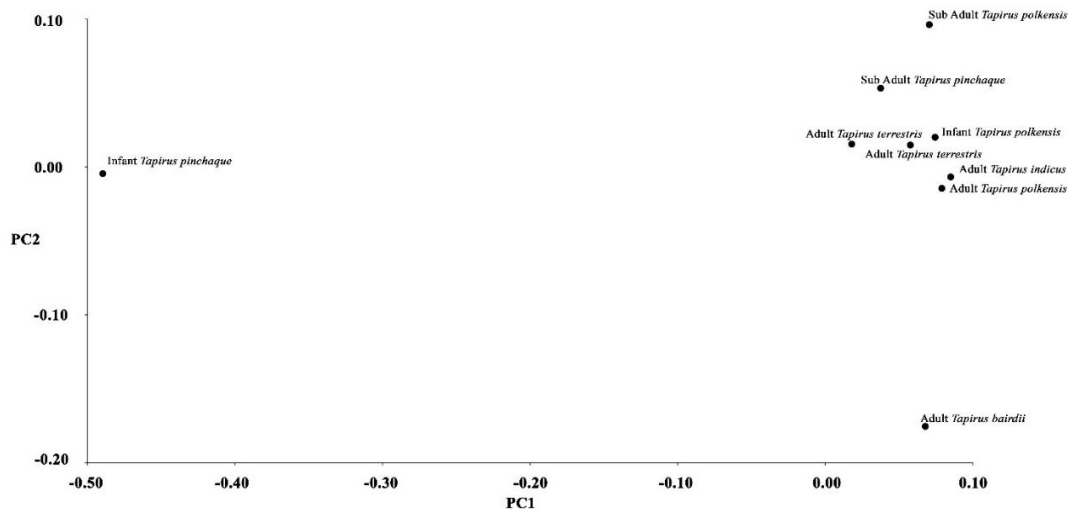


**Figure 9.** Scatterplot graph of PC2 vs. PC1 showing the infant *Tapirus pinchaque* largely accounts for PC1, whereas *Tapirus bairdii* largely accounts for PC2.

**Table 8.** Principle Component Eigenvalues

PC	Eigenvalues	% Variance	Cumulative %
1.	0.03417628	70.952	70.952
2.	0.00550768	11.434	82.387
3.	0.00277967	5.771	88.158
4.	0.00248465	5.158	93.316
5.	0.00138432	2.874	96.190
6.	0.00099233	2.060	98.250
7.	0.00052223	1.084	99.334
8.	0.00032068	0.666	100.000

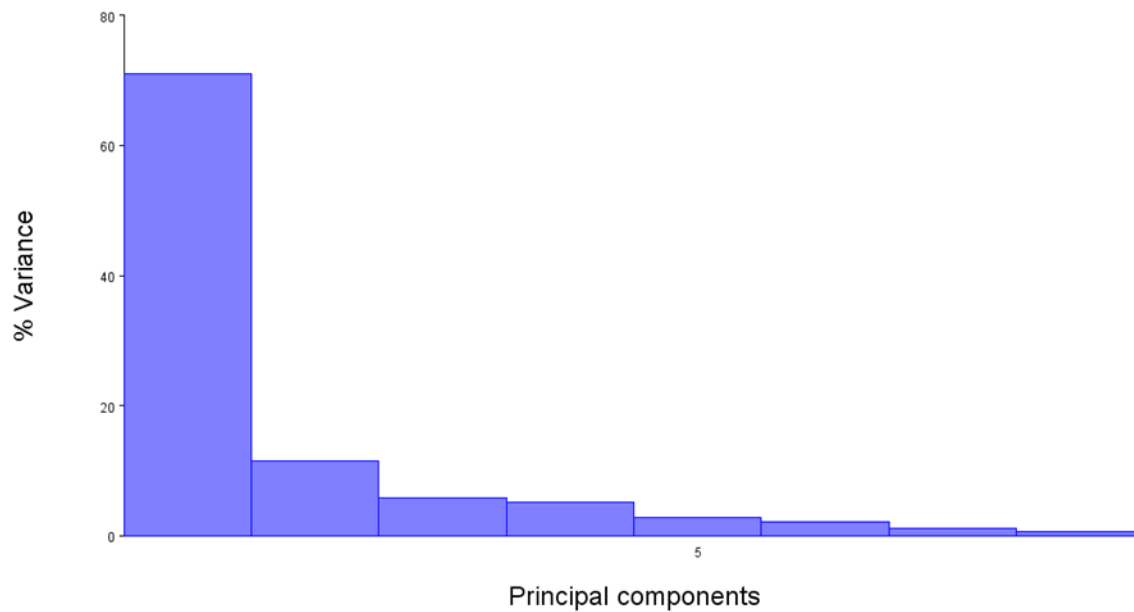


**Figure 10.** Bar graph of the variance attributable to each principle component. Considerably less variation is attributed to PC2, whereas the variation attributable to PC1 is likely the result of missing landmarks.

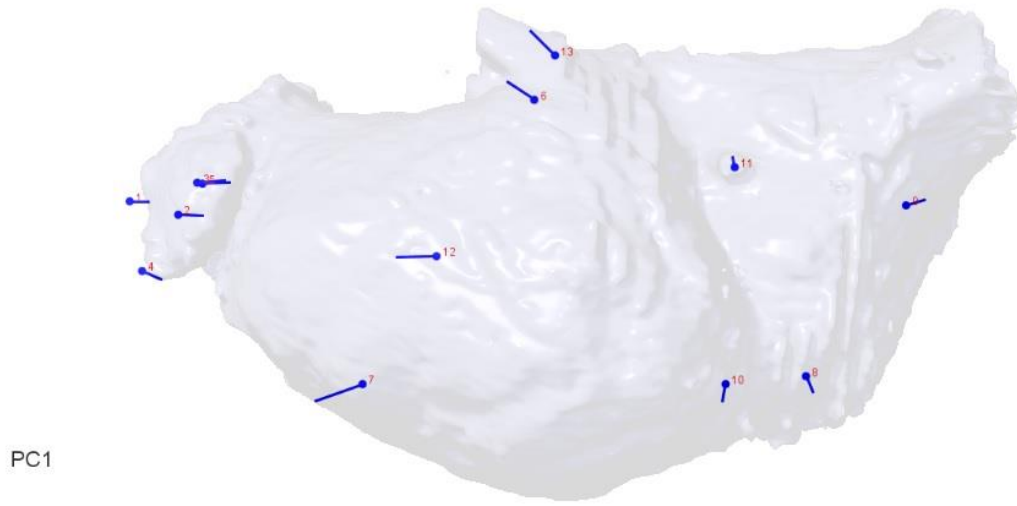


**Figure 11.** Lollipop diagram showing mean shape variation of landmarks for PC1 with transparent endocast of *Tapirus bairdii* (AMNH 80076) oriented along PC1. Points represent the average landmark position, and the stems represent the average vector of variation for each landmark. Vector orientation implies an elongation/truncation of the telencephalon along the antero-posterior orientation.

**Table 9.** Principal Component Coefficients

	PC1	PC2	PC3	PC4	PC5	PC6	PC7	PC8
x1	0.171984	0.058037	0.167248	-0.000943	0.052275	0.092242	0.139606	-0.091483
y1	-0.001387	-0.117569	0.413355	-0.127672	0.059751	0.175867	0.217376	-0.031930
z1	-0.047464	-0.016828	-0.153116	-0.041950	0.010788	-0.014683	0.017072	0.279103
x2	0.226563	0.014424	0.083851	-0.092456	-0.188234	0.102950	0.014365	0.048551
y2	-0.012653	-0.137810	-0.091723	-0.176979	0.051963	0.169037	0.065470	0.285454
z2	0.015912	-0.195923	0.159861	0.048262	0.228951	-0.039317	0.013534	-0.037603
x3	0.255739	-0.186102	-0.339095	0.094523	0.354555	-0.014796	-0.088264	0.019467
y3	0.023338	-0.264443	-0.293849	-0.146480	0.248592	-0.044597	-0.095741	-0.355638
z3	-0.118945	0.077322	0.197895	0.058656	0.086009	-0.076651	-0.227301	-0.001581
x4	0.180258	0.009799	0.052682	-0.182412	-0.177264	-0.170556	-0.135414	-0.220688
y4	-0.081612	0.110452	-0.191588	-0.191802	0.026847	0.103038	-0.282678	0.144229
z4	-0.046201	-0.146172	-0.145070	-0.133490	-0.222822	-0.322685	-0.042532	-0.143589
x5	0.253187	0.009698	0.070964	0.144593	-0.014959	-0.079129	0.029166	0.248927

**Table 9.** Principal Component Coefficients (continued)

	PC1	PC2	PC3	PC4	PC5	PC6	PC7	PC8
y5	0.010983	-0.150459	0.253541	0.299282	-0.255131	-0.176337	0.241740	-0.178095
z5	-0.008836	-0.079267	0.052179	-0.021025	0.048266	0.096429	-0.003104	-0.011815
x6	-0.248669	0.227845	-0.028856	0.165113	0.045833	0.094066	0.215188	-0.242313
y6	0.167212	0.028426	0.168638	0.081459	-0.134524	-0.010769	-0.245430	0.176406
z6	0.183197	-0.004444	-0.144588	0.018671	-0.025004	0.105487	0.420572	-0.154204
x7	-0.438443	-0.512025	-0.069997	0.315227	-0.134172	0.306555	-0.087430	0.061117
y7	-0.161328	0.358198	-0.018752	0.040646	0.067087	-0.137971	-0.212884	-0.256224
z7	0.017975	0.056074	-0.102947	-0.047077	-0.056845	0.067148	0.103351	-0.008792
x8	0.067349	-0.006493	0.021164	0.077683	0.086454	0.308768	-0.167283	-0.198323
y8	-0.146674	0.037062	0.007588	-0.020410	0.181385	-0.076529	-0.066348	-0.098791
z8	0.013208	0.084956	-0.052137	0.060438	-0.006447	-0.016326	0.043807	-0.063634
x9	0.171355	0.029177	-0.066436	0.211948	-0.172070	-0.232474	-0.230569	-0.086167
y9	0.051979	-0.009039	-0.173584	-0.365680	-0.285332	0.105887	0.250310	-0.144620
z9	0.015995	-0.027135	0.013891	-0.031695	0.017770	0.004816	-0.085221	0.088706
x10	-0.029631	0.107605	0.362666	-0.272066	0.383843	-0.076929	0.035331	0.097938
y10	-0.153522	0.097561	0.006871	0.153710	0.217500	0.045663	0.082583	-0.028943
z10	0.016955	0.108359	-0.049192	0.068156	-0.040451	0.105203	-0.038482	-0.005688
x11	-0.015752	0.209318	-0.096490	-0.252294	-0.159386	0.334152	-0.061480	0.043433
y11	0.092360	-0.017126	-0.025562	0.103186	0.026778	-0.132728	-0.017556	0.210380
z11	0.142499	-0.158426	0.134045	-0.042885	0.000543	-0.057326	-0.177039	-0.155121
x12	-0.365295	-0.224093	0.098109	-0.318237	-0.062964	-0.393219	0.099675	0.124148
y12	-0.011649	0.021197	0.058976	0.096304	-0.334730	0.076970	-0.167661	0.130029
z12	-0.201443	0.264616	0.078132	0.109944	-0.065607	0.145699	-0.051298	-0.048268
x13	-0.228646	0.262809	-0.255809	0.109320	-0.013911	-0.271631	0.237107	0.195393
y13	0.222952	0.043551	-0.113913	0.254437	0.129814	-0.097532	0.230821	0.147745
z13	0.017146	0.036868	0.011048	-0.046002	0.024849	0.002207	0.026641	0.262487

### *Discriminant Function Analysis (DFA)*

Extant to Extinct comparisons using DFA result in a procrustes distance of ~0.139, mahalanobis distance of ~1.596, T-square of 5.0274, and a P-value (parametric) of 0.9832 (Table 10). Of the six specimens classified as extant, only five are grouped with the extant specimens whereas one is misclassified as extinct (Table 11). All three of the extinct specimens are correctly classified by the DFA, but after cross-validation, the six extant specimens are classified into three extant members and three extinct members (Table 11). The three extinct specimens are classified into two extant members and one extinct member. High p-values and the dissimilar classification after cross-validation indicate a poor predictive modeling of extinct and extant specimens based on endocranial shape.

**Table 10.** DFA Result

Procrustes distance	0.13874725
Mahalanobis distance	1.5855
T-square	5.0274
P-value (parametric)	0.9832

**Table 11.** DFA Classification/Misclassifications

Extinct/Extant	Extant Allocations	Extinct Allocations
True extant=6	5	1
True extinct=3	0	3
From cross-validation:		
True extant=6	3	3
True extinct=3	2	1

### *Canonical Variance Analysis (CVA)*

The CVA of the infant, sub adult, and adult tapirs in this study results in 75.511% of the variation explained by the first eigenvalue (Table 12). Values for the canonical variates are provided in Table 9. Mahalanobis and Procrustes distances are reported in Tables 13 and 14, and the canonical variates are reported in Table 15. On a plot of CV1 vs CV2, full adult specimens

plot together with a 0.8 confidence ellipse, but no other endocasts of the same ontogenetic stage plot together in morphospace. (Figure 12).

**Table 12.** Canonical Variation Among Groups

	Eigenvalues	% Variance	Cumulative %
CV1	2.36171526	75.511	75.511
CV2	0.76593827	24.489	100.000

**Table 13.** Mahalanobis Distances

	SubAdult	Infant
Infant	2.1466	
Adult	2.7841	2.7010

**Table 14.** CVA Procrustes Distances

	SubAdult	Infant
Infant	0.2904	
Adult	0.1405	0.2837

**Table 15.** Canonical Coefficients

	CV1	CV2
x1	-4.8570	-1.2544
y1	-8.6090	1.3201
z1	8.3290	-2.0391
x2	0.3400	-1.6549
y2	6.5957	-2.5076
z2	-7.4326	2.5637
x3	0.7110	-2.1683
y3	-5.0577	4.0243
z3	-2.8718	3.3511
x4	-3.4924	4.7543
y4	9.2822	-0.4281
z4	0.1546	5.6331
x5	1.6512	-2.6524
y5	-11.1138	1.6173

**Table 15.** Canonical Coefficients (continued)

	CV1	CV2
z5	-2.1577	0.0185
x6	-1.9140	-2.3346
y6	0.1528	-0.0703
z6	-1.3040	-4.7203
x7	-4.3441	-1.5348
y7	-0.0717	2.8696
z7	2.8737	-2.1199
x8	-5.5418	-1.9466
y8	-1.6294	2.7689
z8	0.2457	-1.0140
x9	-1.6797	1.3909
y9	4.0424	-0.7461
z9	1.2551	0.3289
x10	-2.4726	4.5172
y10	-1.0508	-1.5176
z10	1.6817	-2.4989
x11	7.9115	-3.7416
y11	3.0238	-0.9176
z11	-7.5164	4.0894
x12	2.0705	9.0406
y12	2.4927	-1.4569
z12	1.2043	-1.9563
x13	11.6171	-2.4154
y13	1.9426	-4.9559
z13	5.5383	-1.6362

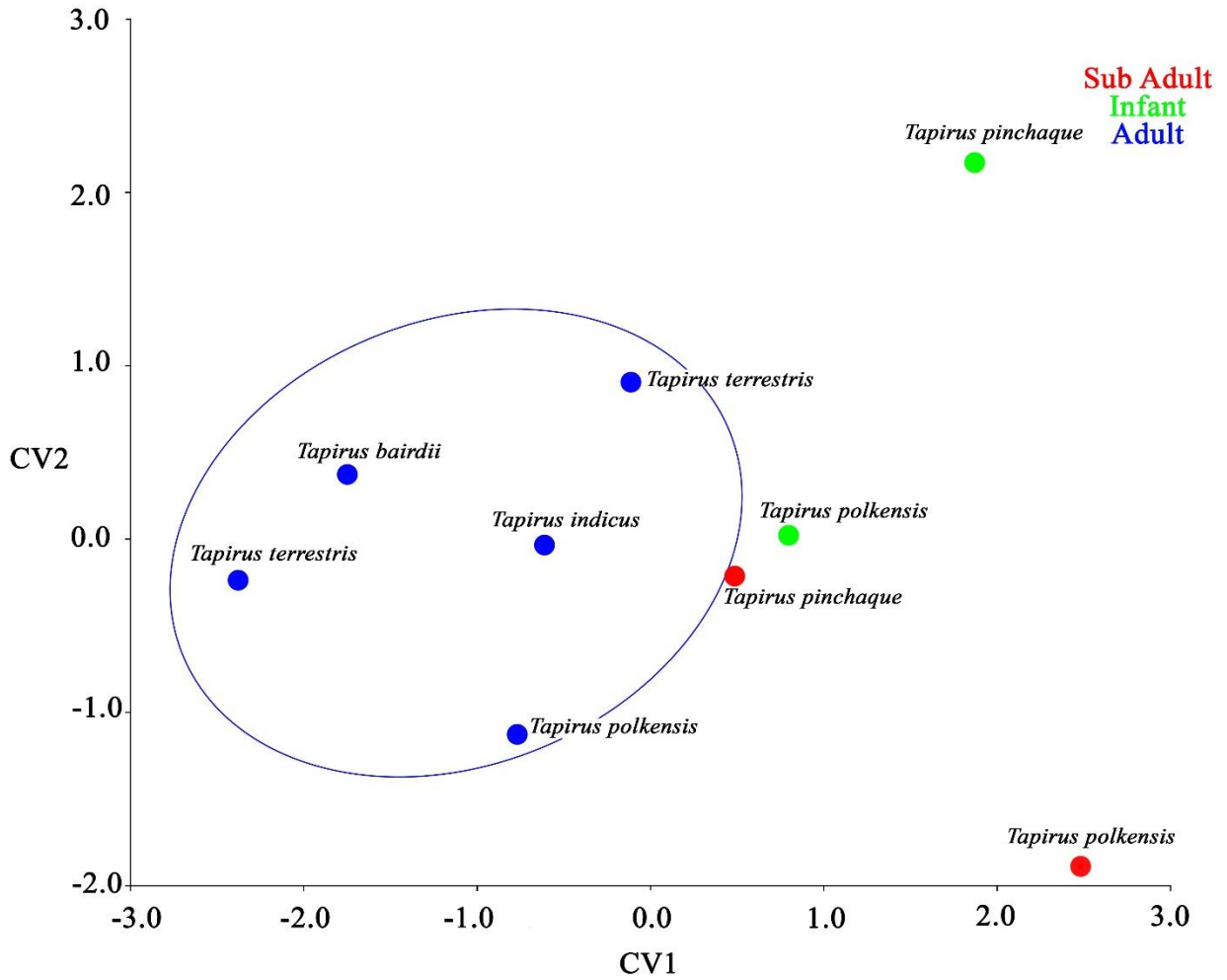


**Figure 12.** Scatterplot of CV1 vs CV2 showing a 0.8 confidence ellipse surrounding the adult specimens in blue. Sub-Adult specimens are represented in red points and the infants are shown in green points.

## CHAPTER 4: DISCUSSION

Much information about an animal's sensory and social ecology is correlated to aspects of brain size and shape (see Torres and Clarke 2018 and Bertrand et al. 2019 for recent examples). It remains possible that factors of skull morphology like adaptations to accommodate mastication musculature and the mobile proboscis coevolved with brain morphology, especially considering the low modularity of the vault in *Tapirus* (Porto et al. 2013). However, the effect of these adaptations on the shape of the brain still can result in a characteristic brain shape that is adapted to carry out neuromuscular functions related to ecology niches in response to sensory stimuli (Bertrand et al. 2019). Upon the discovery of the large accumulation of articulated skeletons of *Tapirus polkensis*, with specimens from all ontogenetic stages, one may consider this as evidence for social behavior as in Currie (1998) and Ibiricu et al. (2013). However, sexual dimorphism is not observed among the tapirs as in the Ashfall specimens of *Teleoceras major* by Mead (2000). Thus, more evidence is needed to support the hypothesis of increased social interactions, or gregarious behavior, by the tapirs from the Gray Fossil Site that results in the large accumulation of articulated skeletons.

PCA shape changes reveal that the most consistent orientation of variation for the landmark configuration is in an inverted lateral perspective (Figure 11). Landmarks 7, 6, 12, and 13 vary along an anterior-posterior vector (Figure 11). These landmarks are associated with the piriform lobe, cruciate sulcus, intersection of the frontal, piriform, and temporal lobes, and the pituitary gland (Table 3). Variation of the hind brain regions appears to vary in dorsal-ventral vectors (landmarks 8, 10, and 11; Figure 11) and an anterior-posterior vector (landmark 9; Figure 11). Hindbrain landmark variation is less than those associated with the telencephalic regions, which supports the use of 3D morphometrics as a better method for measuring endocranial

variation that cannot be detected by gross volumetric measurements, as demonstrated by Bertrand et al. (2019), for example. However, variation in the paleocognition, social ecology, and sensory ecology of *T. polkensis* is not supported by these data without a larger sample size and functional associations with the neuromorphological variation characterized by the PC1 shape changes (Figure 11) and behavior among extant *Tapirus* species. A paleoneurologic investigation of the extinct hyaenid *Pliocrocuta pierrieri* by Vinuesa et al. (2015; 2016) demonstrates the large sample size required for behavioral inferences from endocranial similarity, and how a thorough understanding of brain-behavior correlates among the extant species must be established first, as it is for Hyaenidae by Sakai et al. (2011). Inferences of social ecology based on neural correlates are not broadly applicable among mammals as is the case with sensory ecology (Perez-Barberia et al. 2007; Finarelli and Flynn 2009; Kverková et al. 2018) largely because social behavior is highly nuanced and cannot be considered as simply present or absent (Doody et al. 2012). Ontogenetic variation is established by the CVA (Figure 12) with a confidence ellipse of only 0.8, which is likely the result of the low sample size. Additionally, the brain can change shape throughout ontogeny without regional volume changes (Kawabe et al. 2015), so a neural study of soft tissue *Tapirus* specimens is needed. Additionally, MVZ 124092 does not include the cribriform plates, which define the anterior portion of the endocast and the olfactory bulbs (Macrini et al. 2006). Therefore, shape changes associated with the olfactory region for *T. polkensis* cannot be quantitatively compared to an extant *Tapirus* species and the endocranial ontogeny can only be described qualitatively.

Features characterizing the infant stage cranial endocast of *Tapirus polkensis* indicate a high telencephalic fractional volume and frontal lobe size that decreases during ontogeny, elongation and separation of the olfactory bulbs, and elongation of the endocranial dimensions in

the anterior-posterior direction (Table 4). The sub-adult stage of *Tapirus polkensis* is characterized by medially constricted olfactory bulbs, smaller telencephalic fractional volume, and indistinguishable lobe boundaries within the telencephalon (Figure 6). Reduced hind brain size at the infant stage of *Tapirus polkensis* may lead to hypotheses about the progression of motor coordination because the hind brain functions as the motor cortex (Figure 4) and the *Tapirus* proboscis is comprised of a complex series of muscle tissues (Witmer et al. 1999). Behavioral experimentation with living specimens is needed to test this hypothesis. Low sample size, missing landmarks, and a lack of understanding regarding the functional and morphological variation among extant *Tapirus* endocasts means that this study does not support variation in social behavior as a hypothesis for the large number of *T. polkensis* individuals from the GFS.

Several factors are involved in the variability of brain size in mammals and other vertebrates. Body size and the complexity neurological functioning are examples of a predictive factor in overall brain size (Hofman 1982). Interestingly, body size reductions that constitute a ‘phyletic dwarf’ like *Tapirus polkensis* can result in a disproportionately reduced brain size, resulting in greater encephalized species. (Weston and Lister 2009). Although the authors claim this trend to be applicable to all mammals, cited material within is specific to primate lineages and the differences in late-stage postnatal growth phases (Martin 1983; Shea 1983). Therefore, more research is needed to confirm this trend in other vertebrate groups. Across larger phylogenetic groups (e.g. theropod evolution) gradual reductions in body size over evolutionary time is a contributing factor to increased encephalization (Beyrand et al. 2019). Reduced body size does not appear to be correlated to increased brain size for *Tapirus*. In fact, the conserved EQ values across all specimens presented here suggests that there is no interspecific brain size variation within the genus. Moreover, this conservative EQ condition implies that there is no

variation in the complexity of neurological functioning between extant tapirs and the extinct GFS tapirs.

Social behavior is documented to increase reproductive success in a primate group (Kamil 2004), which could lead to selection pressure for neuromorphological traits related to social living. The positive correlation between brain size and social behavior is contestable, however, with evidence suggesting that a general ecological difference, like diet, is a constraint for brain size evolution (DeCasien et al. 2017). In addition, for the eusocial mammal, *Heterocephalus glaber*, it is internal neural organization that is subject to an individual's role in the group (Holmes et al. 2007), and gross relative size (including neuron count) does not increase among specialized sociality for the eusocial species of Bathyergidae (Kverková et al. 2018). Though the relationship between social behavior and brain size is unresolved in some taxa (for notable exception of brain size and sociality in Carnivora see Perez-Barberia et al. 2007 and Finarelli and Flynn 2009), neural correlations with endocranial patterns and social and sensory ecology can exist. These correlates are documented throughout the animal kingdom mostly as positive correlations between telencephalic fractional volume or whole brain size (e.g. Burish et al. 2004 and Sakai et al. 2011), and problem-solving abilities of Carnivora (e.g. Benson-Amram et al. 2016) or negative correlations as in avian migratory behavior and brain size in which smaller brain sizes are correlated with migratory behavior (e.g. Fuchs et al. 2014). Therefore, if the accumulation of fossil tapirs at the GFS is a signal of increased social interactions, or a larger and cohesive group, then the implication is that there is a selective advantage to this behavior and is accompanied by variation in total relative brain size or the telencephalic region. This is not observed when comparing the endocast shape morphology or the overall relative brain size of *T. polkensis* despite its reduced body size documented in Hulbert et al. (2009). Therefore, the same

sensory and social ecology observed among extant *Tapirus* spp. can be presumed to be consistent with *T. polkensis* of the GFS.

Recently, conservation ecology research outside of paleontology shows that increases in overall relative brain size and extinction rates are correlated (Abelson 2016; Gonzalez et al. 2016). This can be relevant for some extant tapirs considering their endangered status in the 1990s (Downer 1996). It is possible that shifts from metabolic energy expenditures from large brains is shifting to large body size as a mammalian response to human interference with modern environments (Abelson 2016; Gonzalez et al. 2016). However, given that the low coefficient of variation and Z score of *T. polkensis* indicates that the relative brain size of *Tapirus* has remained consistent over the last 5 million years (Table 7), it is unlikely that brain size and body size exhibit changes independently throughout the evolutionary history of the genus.

By studying brain morphology and functioning in extant taxa, paleoneurologists can discuss the implications of what is affected by changes in brain size, shape, and potential confounding factors when interpreting the *Tapirus* endocasts (Early et al. 2020). Neuron cell density and internal circuitry patterns, for example, can be consistent across closely related extant taxa because of phylogeny or convergence (Olkaowicz et al. 2016; Ibáñez et al. 2018). Phylogeny and convergently evolved functional morphology of the brain demonstrates the importance of proper modern analogs when extrapolating behavior from brain size and shape metrics. For example, recent findings about the endocranial morphology of non-volant birds show that they are unique to that of non-avian dinosaurs and cannot serve as a modern analog (Gold and Watanabe 2018) as suggested by a study conducted by Gaetano et al. (2017). The highest measured telencephalic length to width ratio belongs to the double crested cormorant (*Phalacrocorax auritus*) and is qualitatively similar to endocasts of some extinct maniraptors

(Gaetano et al. 2017), but no data on internal neural organization is presented. Information on cellular anatomy from appropriate extant analogs gives functional associations with the differences in relative brain size and shape variation of extinct taxa. Macrì et al. (2019) is an example of a neural architecture study on multiple levels from total volume to the arrangement of cortical neurons of squamates. The authors report correlations with locomotor style on multiple levels of neuroanatomy of the cerebellum and evidence of mosaic-style of brain modifications. Increasing the relative size of a sub region of the brain provides more neurons to process information related to its functional association, which is a cellular origination for Jerison's Principle of Proper Mass (Jerison, 1973). Comparing current understanding of sensory ecology and behavior of *Tapirus* is thus an important step for interpreting the morphology of its endocranial shape.

There is currently little research in the sensory ecology of *Tapirus*. Hunsaker II and Hahn (1965) identify four vocalizations in captive *Tapirus terrestris* that are all associated with functions from pain/threatened responses, exploration, maintaining group cohesion, and aggression. Behavior research on captive *T. bairdii* and *T. indicus* by Gilmore (2007) shows that tapirs spend little time engaging in vocalizations compared to the time spent in exploration via olfaction. Additionally, research by Tortato et al. (2007) of the semi-captive *T. terrestris* reproductive cycle reveals no associative audible vocalizations. This is contradicted by Padilla et al. (2010), in which females vocalizations during courtship are reported for *T. pinchaque*. Recently, vocalizations related to communication between bonding pairs or conflict avoidance are reported from wild *T. bairdii* from Costa Rica (Gómez-Hoyos et al. 2018). Early assertions of Janis (1984) regarding their reliance on olfaction as opposed to vision may be true given the large olfactory bulbs (Figures 5, 6, and 7), but the role of vocalizations in sensory-social ecology

may be as prominent because auditory information shares similar neural integrative pathway as visual information within the brain (Figure 4). These areas are well developed on the *Tapirus* brain (Figures 3, 5, 6, and 7) and thus, auditory information likely plays a significant role in their sensory-social ecology. Understanding species level variation in the sensory integration and behavioral patterns is crucial to this genus level investigation because variation in sensory ecology and behavior gives context to interpret the endocranial shape variation.

Other examples of consistent patterns between external brain morphology and internal organization include the gray and white matter scaling (Zhang and Sejnowski 2000; Harrison et al. 2002). Since white matter scales positively with gray matter as total brain size increases, the observed behavioral and ecological correlations with larger relative brain size like sociality (Perez barberia et al. 2007), problem solving (Benson-Amram et al. 2016), migrating birds (Fuchs et al. 2014), and habitat and social ecology (Shultz and Dunbar 2006) can be reliable based on total brain size. Even brain organization of skates and rays show some evidence of being correlated with habitat complexity that is possibly independent of phylogeny (Lisney et al. 2008). However, it is important to note that the total number of neurons tends to decrease as total brain weights increase among vertebrate taxa (Harrison et al. 2002). Influence of phylogeny on shared avian brain morphology is high (Gold et al. 2018), but not absolutely controlling as is additionally shown by the avian cerebrotypes that are not strictly grouped into established clades (Iwaniuk and Hurd 2005). Based on the results from the present study on tapirs, conserved external morphology and close phylogenetic relationship suggest conserved internal cellular organization throughout the genus.

There are various possibilities to the cause for brain size variation across all mammals. One investigation into the effect of phylogenetic and insular dwarfing on relative brain size

shows that it can result in higher relative brain sizes, but also results in smaller relative brain sizes from limited resources on an island habitat (Weston and Lister 2009). Timing and duration of brain and body growth both pre-and post-natal also play a significant role when examining data from all mammal clades (Sacher and Stefeldt 1974; Barton and Capellini 2011).

Developmental constraints on the endocast by the skull modularity is also a possible controlling factor on brain size and shape (Porto et al. 2013). Skull modularity is a pattern of skull morphology changes that result from regions of the skull changing separately as groups. (i.e. oral, nasal, face, vault, etc). Porto et al. (2013) uses a modularity index which is a number assigned to each defined module. Interestingly to note that the modularity index of the vault (or braincase) from *T. terrestris* (the authors' representative for Perissodactyla) is not significantly correlated, whereas the oral and nasal regions are significantly correlated (Porto et al. 2013). Additionally, these regions have unique osteological and soft tissue modifications that are not present in other perissodactyls (Witmer et al. 1999). Therefore, variation in *Tapirus* brain size and shape may be a secondary result of morphological change from the oral and nasal modules.

The diastema of the *Tapirus* skull extends anteriorly throughout ontogeny and is likely related to the mobile proboscis (Moyanno and Giannini 2017). Overall, the influence of the mobile proboscis of *Tapirus* on skull morphology means that selection for endocranial/brain shape is not driving the morphology of the *Tapirus* endocast and is instead the secondary result of modifications related to the proboscis. However, the present study does not refute the utility of Jerison's Principle of Proper Mass from Jerison (1973). Jerison's principle allows researchers to determine primary sensory modalities from the distribution of brain tissue across the known sensory integration pathways, and it is still commonly cited in modern research (Walsh and

Knoll 2011). Brain morphology through endocast analysis remains a powerful tool for interpreting the behavioral and social ecology of extinct animals that cannot be directly observed.

Endocranial shape observation of the tapirs in this study include large olfaction, so tapirs are integrating large amounts of olfactory stimulus. This is supported by the observations by Montenegro (1998) of *T. terrestris* at mineral licks and by Gilmore (2007) of *T. bairdii* and *indicus* in captivity. Unresolved is the observation of divided olfaction and anterior telencephalic region, which is the condition in all endocasts included in this study. There exists possible links to lateralized olfactory processes that result in separate and unique pathways from the left (emotional processing) and right (memory processing) hemispheres (Royet and Plailly 2004). Unfortunately, cerebral lateralization is more frequently associated with research of human and non-human primate brain-behavior research (e.g. Royet and Plailly 2004 and Uomini and Ruck 2018) and should be considered a more derived structure-function relationship in the mammalian brain; not likely to appear in the perissodactyl lineage. Moreover, the separation of the left and right anterior telencephalon implies a constraint on inter-regional synapse connectivity in the *Tapirus* brain, and possibly inhibits flexible, adaptive responses to sensory stimuli (Brancucci 2012). The anterior telencephalon is most separated in ETMNH 18602 (Figure 5), and the earlier ontogenetic stages of *T. polkensis* are joined (Figures 6 and 7). Neuronal connectivity is most likely greatest in those early stages of development, likely coinciding with the first 6-12 months during which infant extant *Tapirus* spp. stays close to their mother (Downer 1996). Conversely, the internal nasal region of extant species of *Tapirus* shows modifications that result of the functional constraints imposed by a mobile proboscis (modified muscles, nerves, etc.) (Witmer et al. 1999). Just as overall skull morphology is correlated with the presence of the *Tapirus* proboscis, it is likely to presume that divided olfactory bulbs and cerebral cortices are related to a

morphological constraint. The determination of the functional significance and evolutionary origins of divided olfaction is beyond the scope of this thesis and left for future work.

Frontal lobe size among the *Tapirus* endocasts presented here is smaller than the olfactory and auditory processing centers. The function of the frontal lobes for *T. polkensis* likely is consistent with the basal condition (relative to primates and avians), as described by Bucholtz (2012) to be primarily for processing olfactory information as opposed to high order cognitive functions. Evidence from the spatial distribution of DNA harvested from the feces of *T. terrestris* in the Central Amazon suggests no preference for territory overlap among related individuals (Pinho et al. 2014). Although sex and age of the individuals' DNA samples is unknown, a polygamous model of reproduction is established by the evidence from Pinho et al. (2014). Therefore, it is unlikely that neurology of *T. terrestris* (and other members of the genus because of the conserved neuromorphology at the genus level) permits permanent social bonds, which are thought of as more cognitively demanding by Schultz and Dunbar (2006). Using the methods of Zelenitsky et al. (2009), which approximates olfactory acuity in theropods using the olfactory bulb and cerebrum size ratios, it may be possible to measure the increase of olfactory acuity throughout *Tapirus* ontogeny. Experimentation on extant species is needed to confirm the usefulness of olfactory ratios as proxies for olfactory acuity within the genus. In addition, the audio-visual information processing centers (Figure 4) are larger than the frontal lobes in both the modern and extinct specimens (Figures 3 and 5). Therefore, integration of audio-visual senses including olfaction by the frontals, piriform lobes, and olfactory cortices (Royet and Plailly 2004), likely overshadows social signal modulation by the nonapeptide receptors that exist across vertebrates (Huffman et al. 2012). Therefore, any conspecific interactions are likely restricted to impermanent relationships that do not result in cohesive and cooperative social

groups. Given the consistency of the neuromorphological patterns across the genus, it is unlikely that *T. polkensis* exhibits any deviations from the social ecology that is observed in extant members of the genus. With additional samples of *Tapirus* endocasts and sensory-behavioral experimentation on extant species, the behavioral patterns of *T. polkensis* can be reliably modeled after the patterns observed among extant members of the genus.

## CHAPTER 5: CONCLUSIONS

In conclusion, endocranial morphology is a useful testing method for the sensory and behavioral ecology of fossil taxa. The results of this investigation do not indicate interspecific variation for the genus *Tapirus*, and by consequence, there is no support for variation in the complexity of neurological functioning (particularly in the extinct *T. polkensis*). Specifically, *T. polkensis* encephalization falls within the range of extant endocast morphology. Social and sensory ecology is likely present in *Tapirus* evolution for at least 5 Ma based on conserved endocranial morphology. Brain and body size allometry for *Tapirus* does not suggest a tradeoff of brain size for larger body size. Broad correlations between brain size and extinction/endangerment status from Abelson (2016) and Gonzalez et al. (2016) may not appear on the genus-level with low sample size, despite temporal separation. Based on the presented data, it is likely that both extant and extinct species of *Tapirus* exhibit similar patterns of behavior in life. More behavioral and sensory ecology research of extant *Tapirus* ssp. is needed to test conclusions regarding variation in brain shape morphology for *Tapirus*. Finally, larger sample size and a more taxonomically diverse dataset can broaden our understanding of the evolution of social behavior, sensory ecology, and the neural correlates for *Tapirus*.

## REFERENCES

- Abelson, ES. 2016. Brain size is correlated with endangerment status in mammals. *Proceedings of the Royal Society-Biology*. 283: 20152772
- Ahrens, HE. 2014. Morphometric study of phylogenetic and ecologic signals in procyonid (Mammalia: Carnivora) endocasts. *The Anatomical Record*. 297: 2318-2330
- Balanoff, AM., Bever, GS., Rowe, TB., Norell, MA. 2013. Evolutionary origins of the avian brain. *Nature*. 501: 93-96.
- Balanoff AM., Bever GS., Norell MA. 2014. Reconsidering the avian nature of the oviraptorosaur brain (Dinosauria: Theropoda). *PLoS ONE*. 9(12): e113559.
- Balanoff AM., Smaers, JB., Turner, AH. 2015. Brain modularity across the theropod-bird transition: testing the influence of flight on neuroanatomical variation. *Journal of Anatomy*. 229: 204-214.
- Barton, RA., Capellini, I. 2011. Maternal investment, life histories, and the costs of brain growth in mammals. *PNAS*. 108(15): 6169-6174.
- Benson-Amram, S., Dantzer B., Stricker, G, Swanson, EM., Holekamp, KE. 2016. Brain size predicts problem-solving ability in mammalian carnivores. *PNAS*. 113(9): 2532-2537.
- Bertrand, O.C. Martin-Flores, G., Silcox, M.T. 2019. Endocranial shape variation in the squirrel-related clade and their fossil relatives using 3D geometric morphometrics: contributions of locomotion and phylogeny to brain shape. *Journal of Zoology*. 308(3): 197-211.
- Beyrand, V., Voeten, DFAE., Bureš, S., Fernandez, V., Janáček, J., Jirák, D., Rauhut, O., Tafforeau, P. 2019. Multiphase progenetic development shaped the brain of flying archosaurs. *Scientific Reports*. 9: 1-15.
- Boessenecker, RW., Ahmed, E., Geisler, JH. 2017. New records of the dolphin *Albertocetus*

- meffordorum* (Odontoceti: Xenorophidae) from the lower Oligocene of South Carolina: Encephalization, sensory anatomy, postcranial morphology, and ontogeny of early odontocetes. *PLoS ONE* 12(11): e0186476.
- Boddy, AM., McGowen, MR., Sherwood, CC., Grossman, LI., Goodman, M., Wildman, DE. 2012. Comparative analysis of encephalization in mammals reveals relaxed constraints on anthropoid primate and crustacean brain scaling. *Journal of Evolutionary Biology*. 25: 981-994.
- Bookstein, FL. 1991. *Morphometric tools for landmark data: Geometry and biology*. Cambridge: Cambridge University Press.
- Brancucci, A. 2012. Neural correlates of cognitive ability. *Journal of Neuroscience Research*. 90(7): 1299-1309.
- Buchholtz, E. 2012. Dinosaur paleoneurology. In *The complete dinosaur*. Brett-Surman, MK., Holtz, TR., Farlow, JO. (Eds.). Indiana University Press. 191-208.
- Burish, MJ., Kueh, HY., Wang, SSH. 2004. Brain Architecture and Social Complexity in Modern and Ancient Birds. *Brain, Behavior, and Evolution*. 63: 107-124.
- Burger, JR., George, MA., Leadbetter, C., Shaikh, F. 2019. The allometry of brain size in mammals. *Journal of Mammalogy*. 100(2): 276-283.
- Butler, AB., Manger, PR., Lindahl, BIB., Århem, P. 2005. Evolution of the neural basis of consciousness: a bird–mammal comparison. *Bioessays*. 27(9): 923-936.
- Colbert, MW. 1999. Patterns of evolution and variation in the Tapiroidea (Mammalia: Perissodactyla) (*Doctoral dissertation*). The University of Texas at Austin, Texas.
- Currie, PJ. 1998. Possible evidence of gregarious behavior in tyrannosaurids. *Gaia*. 15: 271-277.
- DeCasien, A. R., Williams, S. A., Higham, J. P. 2017. Primate brain size is predicted by diet but

- not sociality. *Nature ecology & evolution*. 1(5): 1-7.
- Domínguez Alonso P, Milner AC, Ketcham RA, Cookson MJ, Rowe TB. 2004. The avian nature of the brain and inner ear of Archaeopteryx. *Nature*. 43: 666-669.
- Doody, J. S., Burghardt, G. M., Dinets, V. 2013. Breaking the social–non-social dichotomy: a role for reptiles in vertebrate social behavior research?. *Ethology*. 119(2): 95-103.
- Downer, C. 1996. The mountain tapir, endangered ‘flagship’ species of the high Andes. *Oryx*. 30(1): 45-58.
- Dragonfly 4.1 [Computer software]. Object Research Systems (ORS) Inc, Montreal, Canada, 2019; software available at <http://www.theobjects.com/dragonfly>.
- Durrleman, S., Pennec, X., Trouvé, A., Ayacöe, N., Braga, J. 2012. Comparison of the endocranial ontogenies between chimpanzees and bonobos via temporal regression and spatiotemporal registration. *Journal of Human Evolution*. 62: 74-88.
- Dunn, RH. 2018. Functional Morphology of the Postcranial Skeleton. In. *Methods in Paleoecology*. Eds. Croft, DA., Su, DF., Simpson, SW. *Springer Nature*. Switzerland.
- Early, CM., Ridgely, RC., Witmer., LM. 2020. Beyond endocasts: using predicted brain structure volumes of extinct birds to assess neuroanatomical and behavior inferences. *Diversity*. 12(1): 34.
- Finarelli, JA., Flynn, JJ. 2009. Brain-size evolution and sociality in Carnivora. *PNAS*. 106(23): 9345-9349.
- Franzosa, J. 2004. Evolution of the brain in Theropoda (*Doctoral dissertation*). The University of Texas at Austin, Texas.
- Fuchs, R., Winkler, H., Bingman, VP., Ross, JD., Bernroider, G. (2014) Brain Geometry and its Relation to Migratory Behavior in Birds. *Journal of Advanced Neuroscience Research*. 1:

1-9.

- Funston, GF., Currie, PJ., Eberth, DA., Ryan, MJ., Chinzorig, T., Badamgarav, D., Longrich, N. R. 2016. The first oviraptorosaur (Dinosauria: Theropoda) bonebed: evidence of gregarious behaviour in a maniraptoran theropod. *Scientific Reports*. 6: 35782.
- Gaetano, TM., Yacobucci, MM., Bingman, VP. 2017. On the paleontology of animal cognition: using the brain dimensions of modern birds to characterize maniraptor cognition. *Journal of Advanced Neuroscience Research*. Special Issue: 12-17.
- Gilmore, M. 2007. Tapir behavior – an examination of activity patterns, mother young interactions, spatial use, and environmental effects in captivity on two species (*Tapirus indicus* & *Tapirus bairdii*). *Master's Thesis*. Oregon State University, Oregon.
- Gold, MEL., Watanabe, A. 2018. Flightless birds are not neuroanatomical analogs of non-avian dinosaurs. *BMC Evolutionary Biology*. 18(190): 1-11.
- Gómez-Hoyos, DA., Escobar-Lasso, S., Brenes-Mora, E., Schipper, J., González-Maya, JF. 2018. Interaction behavior and vocalization of the baird's tapir *Tapirus bairdii* from Talamanca, Costa Rica. *Neotropical Biology and Conservation*. 13(1): 17-23.
- Gonzalez, A., González, M., Vilà, C., Revilla, E. 2016. Larger brain size indirectly increases vulnerability to extinction in mammals. *Evolution*. 70(6): 1364-1375.
- Gunz, P., Neubauer, S., Golovanova, L., Doroniechev, V., Maureille, B., Hublin, J. 2012. A uniquely modern human pattern of endocranial development. Insights from a new cranial reconstruction of the Neandertal newborn from Mezmaiskaya. *Journal of Human Evolution*. 62: 300-313.
- Harrison, KH., Hof, PR., Wang, SS. 2002. Scaling laws in the mammalian neocortex: does form provide clues to function? *Journal of Neurocytology*. 31: 289-298.

- Hart, BL., Hart, LA., Pinter-Wollman, N. 2008. Large brains and cognition: where do elephants fit in? *Neuroscience and Biobehavioral Reviews*. 32: 86-98.
- Hofman, MA. 1982. A two-component theory of encephalization in mammals. *Journal of Theoretical Biology*
- Holden, J., Yanuar, A., Maryr, D., (2003) The Asian Tapir in Kerinci Seblat National Park, Sumatra: evidence collected through photo-trapping. *Oryx*. 37(1): 34-40.
- Holmes, MM., Rosen, GJ., Jordan, CL., de Vries, GJ., Goldman, BD., Forger, NG. 2007. Social control of brain morphology in a eusocial mammal. *PNAS*. 104(25): 10548-10552
- Huffman, LS., O'Connell, LA., Kenkel, CD., Kline, RJ., Khan, IA., Hofmann, HA. 2012. Distribution of nonapeptide systems in the forebrain of an African cichlid fish, *Astatotilapia burtoni*. *Journal of Chemical Neuroanatomy*. 44: 86-97.
- Hulbert, RC., Wallace, SC., Klippel, WE., Parmalee, PW. 2009. Cranial morphology and systematics of an extraordinary sample of the Late Neogene dwarf tapir, *Tapirus polkensis* (Olsen). *Journal of Paleontology*. 83(2): 238-262.
- Hunsaker II, D., Hahn, TC. 1965. Vocalization of the South American tapir, *Tapirus terrestris*. *Animal Behavior*. 13(1): 69-74.
- Ibáñez, CG., Iwaniuk, AN., Wylie, DR. 2018. Parrots have evolved a primate-like telencephalic-midbrain-cerebellar circuit. *Scientific Reports*. 8(9960): 1-11.
- Ibiricu, LM., Martínez, RD., Casal, GA., Cerda, IA. 2013. The behavioral implications of a multi-individual bonebed of a small theropod dinosaur. *PLoS ONE*. 8(5): 1-11.
- Iwaniuk, AN., Nelson, JE. 2002. Can endocranial volume be used as an estimate of brain size in birds. *Canadian Journal of Zoology*. 80: 16-23

- Iwaniuk, AN., Hurd, PL. 2005. The evolution of cerebrotypes in birds. *Brain Behavior and Evolution*. 65: 215-230.
- Iyengar, S., Parishar, P., Mohapatra, AN. 2017. Avian cognition and consciousness—from the perspective of neuroscience and behavior. In *Self, Culture, and Consciousness*. Menon et al. (eds). Springer Nature, Singapore. 23-50.
- Jacobs, I., Kabadayi, C., Osvath, M. 2019. The development of sensorimotor cognition in common ravens (*Corvus corax*) and its comparative evolution. *Animal Behavior and Cognition*. 6(3): 194-212.
- Janis, C. 1984. Tapirs as living fossils. In: Eldredge, N., Stanley, S. Eds. *Living Fossils*. Springer-Verlag. New York.
- Jerison, HJ. 1973. The evolution of the brain and intelligence. London. *Academic Press*.
- Jerison, HJ. 1985. Animal intelligence as encephalization. *Philosophical Transactions of the Royal Society of London. Series B, Biological Sciences*. 308(1135): 21-35.
- Kamil, AC. 2004. Sociality and the evolution of intelligence. *Trends in Cognitive Sciences*. 8(5): 195-197.
- Kawabe, S., Matsuda, S., Tsunekawa, N. and Endo, H. 2015. Ontogenetic shape change in the chicken brain: implications for paleontology. *PLoS One*. 10(6): 1-16.
- Keeler, JF., Robbins, TW. 2011. Translating cognition from animals to humans. *Biochemical pharmacology*. 81(12): 1356-1366.
- König, HE., Liebich, HG., Červený, C. 2009. Nervous system (systema nervosum). In: *Vertebrate Anatomy of Domestic Mammals*. 4<sup>th</sup> Edition. Eds. König, HE., Liebich, HG. Schattauer. Stuttgart New York. 489-561.
- Klingenberg, C. P. 2011. MorphoJ: an integrated software package for geometric

- morphometrics. *Molecular Ecology Resources*. 11: 353-357
- Kverková, K., Belíková, T., Olkowicz, S., Pavelková, Z., O'Riain, MJ., Šumbera, R., Burda, H., Bennett, NC., Němec, P. 2018. Sociality does not drive the evolution of large brains in eusocial African mole-rats. *Scientific Reports*. 8: 1-14.
- Lautenschlager, S., Rayfield, E., Altangerel, P., Zanno, L., and Witmer, L. 2012. The endocranial anatomy of Therizinosauria and its implications for sensory and cognitive function. *PLoS ONE*. 7(12): e52289.
- Lisney, TJ., Yopak, KE., Montgomery, JC., Collin, SP. 2008. Variation in brain organization and cerebellar foliation in Chondrichthyans: Batoids. *Brain, Behavior, and Evolution*. 72: 262-282.
- Logan, CJ., Avin, S., Boogert, N., Buskell, A., Cross, FR., Currie, A., Jelbert, S., Lukas, D., Mares, R., Navarrete, AF., Shigeno, S., Montgomery, SH. 2018. Beyond brain size: uncovering the neural correlates of behavioral and cognitive specialization. *Comparative Cognition & Behavior Reviews*. 13: 55-89.
- Lyras, GA., Van Der Geer, AEA. 2003. External brain anatomy in relation to the phylogeny of Caninae (Carnivora: Canidae). *Zoological Journal of the Linnean Society*. 138: 505-522.
- Macrì, S., Savriama, Y., Khan, I., Di-Poi, N. 2019. Comparative analysis of squamate brains unveils multi-level variation in cerebellar architecture associated with locomotor specialization. *Nature Communications*. 10(1): 1-16.
- Macrini, TE., Rowe, T., Archer, M. 2006. Description of a cranial endocast from a fossil platypus, *Obdurodon dicksoni* (Monotremata, Ornithorhynchidae), and the relevance of endocranial characters to monotreme monophyly. *Journal of Morphology*. 267: 1000-1015.

- Macrini, TE., Rougier, GW., Rowe, T. 2007a. Description of a cranial endocast from the fossil mammal *Vincelestes neuquenianus* (Theriiformes) and its relevance to the evolution of endocranial characters in therians. *The Anatomical Record*. 290: 875-892.
- Macrini, TE., Rowe, T., VandeBerg, JL. 2007b. Cranial endocasts from a growth series of *Monodelphis domestica* (Didelphidae, Marsupialia): a study of individual and ontogenetic variation. *Journal of Morphology*. 268: 844-865.
- Martin, R. D. 1983. *Human Brain Evolution in an Ecological Context: 52nd James Arthur Lecture on the Evolution of the Human Brain*. American Museum of Natural History. New York.
- Mead, A. 2000. Sexual dimorphism and paleoecology in *Teleoceras*, a North American Miocene rhinoceros. *Paleobiology*. 26(4): 689-706.
- Melhorn, J., Hunt, GR., Gray, RD., Rehkämper, G., Güntürkün, O. 2010. Tool-making new Caledonian crows have large associative brain areas. *Brain, Behavior, and Evolution*. 75: 63–70
- Mihlbachler, MC. 2003. Demography of late Miocene rhinoceroses (*Teleoceras proterum* and *Aphelops malacorhinus*) from Florida: linking mortality and sociality in fossil assemblages. *Paleobiology*. 29(3): 412-428.
- Montenegro, O. L. 1998. The behavior of lowland tapir (*Tapirus terrestris*) at a natural mineral lick in the Peruvian Amazon. *Master's Thesis*. University of Florida, Florida.
- Moyano, SR., Giannini, NP. 2017. Comparative cranial ontogeny of *Tapirus* (Mammalia: Perissodactyla: Tapiridae). *Journal of Anatomy*. 231: 665-682.

- Neubauer, S., Gunz, P., Hublin, J. 2010. Endocranial shape changes during growth in chimpanzees and humans: A morphometric analysis of unique and shared aspects. *Journal of Human Evolution*. 59: 555-566.
- Nomura, T., Izawa, E. 2017. Avian brains: insights from development, behavior and evolution. *Development, Growth, and Differentiation*. 59: 244-257.
- Olkowicz, S., Kocourek, M., Lučan, RK., Porteš, M., Tecumseh, W., Herculano, S., Němec, P. 2016. Birds have primate-like numbers of neurons in the forebrain. *PNAS*. 113(26): 7255-7260.
- Perez-Barbaria, FJ., Shultz, S., Dunbar, RIM. 2007. Evidence for the coevolution of sociality and relative brain size in three orders of mammals. *Evolution*. 6(12). 2811-2821.
- Padilla, M., Dowler, RC., Downer, CC. 2010. *Tapirus pinchaque* (Perissodactyla: Tapiridae). *Mammalian Species*. 42(863): 166-182.
- Pinho GM, Goncalves da Silva A, Hrbek T, Venticinque EM, Farias IP. 2014. Kinship and Social Behavior of Lowland Tapirs (*Tapirus terrestris*) in a Central Amazon Landscape. *PLoS ONE*. 9(3): e92507.
- Porto, A., Shirai, LT., de Oliveira, FB., Marroig, G. 2013. Size variation, growth strategies, and the evolution of modularity in the mammalian skull. *Evolution*. 67(11): 3305-3322.
- Proffitt, JV., Clarke, JA., Scofield, RP. 2016. Novel insights into early neuroanatomical evolution in penguins from the oldest described penguin brain endocast. *Journal of Anatomy*. 229: 228-238.
- Rogers, S. W. 2005. Reconstructing the behaviors of extinct species: an excursion into comparative paleoneurology. *American Journal of Medical Genetics Part A*. 134(4): 349-356.

- Rose, J., Colombo, M. 2005. Neural correlates of executive control in the avian brain. *PLoS Biology*. 3(6): e190.
- Rowe, T., Macrini, T., Luo, Z. 2011. Fossil evidence on the origin of the Mammalian brain. *Science*. 330(6032): 955-957.
- Royet, JP., Plailly, J. 2004. Lateralization of olfactory processes. *Chemical Senses*. 29(8): 731-745.
- Sacher, GA., Staffeldt, EF. 1974. Relation of gestation time to brain weight for placental mammals: implications for the theory of vertebrate growth. *The American Naturalist*. 108(963): 593-615
- Sakai, ST., Arsznov, BM., Lundrigan, BL., Holekamp, KE. 2011. Brain size and social complexity: a computed tomography study in Hyaenidae. *Brain, Behavior, and Evolution*. 77(2): 91-104.
- Sampson, S.D., Witmer, L.M. 2007. Craniofacial anatomy of *Majungasaurus crenatissimus* (Theropoda: Abelisauridae) from the Late Cretaceous of Madagascar. *Society of Vertebrate Paleontology Memoir 8 Journal of Vertebrate Paleontology*. 27(2): 32–102.
- Sanders, RK., Smith, DK. 2005. The endocranium of the theropod dinosaur *Ceratosaurus* studied with computed tomography. *Acta Palaeontologica Polonica*. 50: 601-616.
- Seed, A., Emery, N., Clayton, N. 2009. Intelligence in corvids and apes: a case of convergent evolution? *Ethology*. 115: 401-420.
- Schubert, BW., Mead, JI. 2011. *Gray Fossil Site: 10 Years of Research*. Johnson City, Tennessee. Don Sundquist Center of Excellence in Paleontology, East Tennessee State University.
- Shea, B. T. 1983. Phyletic size change and brain/body allometry: A consideration based on the African pongids and other primates. *International Journal of Primatology*. 4(1): 33-62.

- Shultz, S., Dunbar, RIM. 2006. Both social and ecological factors predict ungulate brain size. *Proceedings of the Royal Society Biology*. 273: 207-215.
- Tobler, MW. 2008. The ecology of the lowland tapir in Madre de Dios, Peru: Using new technologies to study large rainforest mammals. *Doctoral Dissertation*. Texas A&M University, Texas.
- Torres, CR., Clarke, JA. 2018. Nocturnal giants: evolution of the sensory ecology in elephant birds and other palaeognaths inferred from digital brain reconstructions. *Proceedings of the Royal Society-Biology*. 285(1890): 20181540
- Tortato, MA., Oliveira, LG., Filho, LC., Brusius, L., Hötzel, MJ. 2007. Reproductive behavior repertoire of semi-captive lowland tapir *Tapirus terrestris* (Linnaeus, 1758). *Biotemas*. 20(4): 135-139.
- Tucker, ST., Otto, RE., Joeckel, RM., Voorhies, MR. 2014. The geology and paleontology of Ashfall Fossil Beds, a late Miocene (Clarendonian) mass-death assemblage, Antelope County and adjacent Knox County, Nebraska, USA. In Korus, JT. *Geologic Field Trips along the boundary between the Central Lowlands and Great Plains: 2014 Meeting of the GSA North-Central Section*. 1-22. Boulder, Colorado. The Geological Society of America.
- Uomini, NT., Ruck, L. 2018. Manual laterality and cognition through evolution: an archaeological perspective. In *Progress in Brain Research*. Eds. Forrester, GS., Hopkins, WD., Hudry, K., Lindell, A. 238: 295-323.
- Varricchio, DJ., Sereno, PC., Xijin, Z., Lin, T., Wilson, JA., Lyon, GH. 2008. Mud-trapped herd captures evidence of distinctive dinosaur sociality. *Acta Palaeontologica Polonica*. 53(4): 567-578.

- Vinuesa, V., Madurell-Malapeira, J., Fortuny, J., Alba, D. M. 2015. The Endocranial morphology of the Plio-Pleistocene bone-cracking hyena *Pliocrocuta perrieri*: Behavioral implications. *Journal of Mammalian Evolution*, 22(3): 421-434.
- Vinuesa, V., Iurino, DA., Madurell, J., Liu, J. Fortuny, J., Sardella, R., Alba, DM. 2016. Inferences of social behavior in bone-cracking hyaenids (Carnivora, Hyaenidae) based on digital paleoneurological techniques: Implications for human-carnivoran interactions in the Pleistocene. *Quaternary International*. 413: 7-14.
- Walker, EP. 1964. Mammals of the world. vol. 2. Baltimore. *John Hopkins Press*.
- Walsh SA., Knoll, F. 2011. Directions in palaeoneurology. *Special Papers in Palaeontology*. 86: 263-279.
- Walsh, SA., Knoll, F. 2018. The evolution of avian intelligence and sensory capabilities: the fossil evidence. In *Digital Endocasts. Replacement of Neanderthals by Modern Humans Series*. Eds. Brunner, E., et al. *Springer*. Japan. 59-69.
- Weston, EM., Lister, AM. 2009. Insular dwarfism in hippos and a model for brain size reduction in *Homo floresiensis*. *Nature*. 459(7243): 85-88.
- Witmer, LM., Sampson, SD., Solounias, N. 1999. The proboscis of tapirs (Mammalia: Perissodactyla): a case study in novel narial anatomy. *Journal of Zoology*. 249(3): 249-267.
- Zelenitsky, D., Therrian, F., Ridgely, R., McGee, A., and Witmer, L. 2011. Evolution of olfaction in non-avian theropod dinosaurs and birds. *Proceedings of the Royal Society Biology*. 278: 3625-3634.
- Zhang, K., Sejnowsk., TJ. 2000. A universal scaling law between gray matter and white matter of cerebral cortex. *PNAS*. 97(10): 5621-5626.

## VITA

THOMAS M. GAETANO

- Education: M.S. Geosciences (Paleontology), East Tennessee State University, Johnson City, Tennessee, 2020
- B.S. Geology (Paleobiology), Bowling Green State University, Bowling Green, Ohio, 2016
- Public Schools, Wellington, Ohio
- Professional Experience: Graduate assistant/coordinator, East Tennessee State University, College of Arts and Sciences, 2019-2020.
- Gray Fossil Site volunteer and outreach, event planning team, field crew; Johnson City, Tennessee, 2018-2020
- Tutor, East Tennessee State University, College of Arts and Sciences 2018-2019.
- Temporary Support, Gray Fossil Site; Johnson City, Tennessee, 2019.
- Charter School Guest Educator, Enriched Schools; Nashville, Tennessee, 2018.
- Public School Substitute Teacher, Wood County Educational Services, Bowling Green, Ohio, 2017.
- Internship, Ashfall Fossil Beds; Royal, Nebraska, 2013, 2016.

Tutor at Student Athletic Services, Bowling Green, Ohio,  
2014-2016.

Publications: Gaetano, TM., Yacobucci, MM., Bingman, VP. (2017) On the  
paleontology of animal cognition: using the brain  
dimensions of modern birds to characterize maniraptor  
cognition. *Journal of Advanced Neuroscience Research*.  
Special Issue. 12-19.

Presentations: Behavioral implications of relative brain size in the extinct  
dwarf Tapir, *Tapirus polkensis*. American Society of  
Mammalogists, 2019.

Futurism in paleontology: applications of 3D spatial data from  
the Gray Fossil Site to a visual framework for research  
and exhibits. Association for Materials and Methods in  
Paleontology, 2019.

Anatomical markers for elevated cognition in dinosaurs.  
BGSU Undergraduate Symposium for Research and  
Scholarship, 2016.

Honors and Awards: Best New Graduate Student, 2019  
Mancusso Field Studies Scholarship, 2015  
Lougheed Scholarship, 2013  
Forsyth Award, 2012  
Presidential Scholar Award, 2012  
Buckeye Boys' State attendee, 2011

AFFILIATIONS

2019-Current	Association for Materials and Methods in Paleontology
2019-Current	American Society of Mammalogists
2018-Current	Society of Vertebrate Paleontology
2014-2016	Sigma Gamma Epsilon